Electronic Supplementary Material (ESI) for Organic Chemistry Frontiers.

Supporting information for

Coordination assembly and NIR photothermal conversion of Cp*Rh-based supramolecular topologies based on distinct conjugated systems

Li-Long Dang‡*[ac], Ting-Ting Zhang‡[ab], Tian Chen[a], Ying Zhao[a], Chen-Chen Zhao[a], Francisco Aznarez[c], Kai-Xin Sun[a], Lu-Fang Ma[ab]

a. College of Chemistry and Chemical Engineering, Henan Province Function-Oriented Porous Materials Key Laboratory, Luoyang Normal University, Luoyang 471934, P. R. China.

b. College of materials and Chemical Engineering, China Three Gorges University, Yichang 443002, P. R. China.

c. Shanghai Key Laboratory of Molecular Catalysis and Innovative Materials; State Key Laboratory of Molecular Engineering of Polymers, Department of Chemistry, Fudan University, Shanghai 200438, P. R. China.
*E-mail: danglilong8@163.com

Contents

1. General considerations **2**

2. Synthesis of complex 1a, 1b, 2, 3, 4, 5, 6, 7 **2**

3. NMR spectra **5**

4. ESI-MS spectra **29**

5. UV-vis spectra **33**

6. Near-infrared photothermal conversion research **34**

7. X-ray crystallography details **36**

8. References **44**

1. General considerations

All reagents and solvents were purchased from commercial sources and used as supplied unless otherwise mentioned. The starting materials $[Cp^*RhCl_2]_2$ ($Cp^*=\eta^5$-pentamethylcyclopentadienyl)[1], BiBzIm (BiBzIm = 2, 2′-bisbenzimidazole)[2] were prepared by literature methods. NMR spectra were recorded on Bruker AVANCE I 400 spectrometers at room temperature and referenced to the residual protonated solvent. Proton chemical shifts are reported relative to the solvent residual peak (δ H = 3.31 (CD_3OD), 2.50 (DMSO-D6), 1.96 (CD_3CN), 2.75, 2.92 (DMF))). Coupling constants are expressed in Hertz. Elemental analyses were performed on an Elementar Vario EL III analyzer. ESI-MS spectra were recorded on a Micro TOF II mass spectrometer.

2. Synthesis of complexes 1a, 1b, 2, 3, 4, 5, 6, 7

Preparation of complex 1a (Borromean ring)

AgOTf (123.2 mg, 0.48 mmol) was added to a solution of $[Cp^*RhCl_2]_2$ (74.4 mg, 0.12 mmol) in a CH_3OH (10 mL) at room temperature. The mixture was stirred in the dark for 24 h and then filtered. 5,8-Dihydroxy-1,4-naphthoquinone (22.8 mg, 0.12 mmol) and NaOH (9.6 mg, 0.24 mmol) were added to the filtrate. The mixed solution was stirred at room temperature for 12 h to give a green solution. **L1** (25.2 mg, 0.12 mmol) was added to the solution. The mixture was stirred at room temperature for another 12 h to give a dark green solution. Upon the addition of diethyl ether, a dark green solid was precipitated and collected. The product was recrystallized from a CH_3OH/diethyl ether mixture to afford green block-shaped crystals (**1a**). 121.63 mg, yield 88.2%. Anal. Calcd for $C_{264}H_{264}N_{24}O_{60}F_{36}S_{12}Rh_{12}$ (M = 7036.69): C, 45.06; H, 3.80; N, 4.8. Found: C, 45.01; H, 3.70; N, 4.60. ^1H NMR (500 MHz, CD_3OD, ppm, with respect to Cp*Rh): δ = 9.36 (d, 4H J=6.0 Hz, pyridyl-aH), δ = 7.46 (d, 4H, J = 6.0 Hz, 4H, pyridyl-bH), δ= 6.51 (s, 4H, phenyl-dH of E4), δ = 5.10 (s, 2H, cH of -CH=N- group), δ = 1.71 (s, 30H, Cp*-H).

Preparation of complex 1b

AgOTf (123.2 mg, 0.48 mmol) was added to a solution of $[Cp^*RhCl_2]_2$ (74.4 mg, 0.12 mmol) in a CH_3CN (10 mL) at room temperature. The mixture was stirred in the dark for 24 h and then filtered. 5, 8-Dihydroxy-1,4-naphthoquinone (22.8 mg, 0.12 mmol) and NaOH (9.6 mg, 0.24 mmol) were added to the filtrate. The mixed solution was stirred at room temperature for 12 h to give a green solution. **L1** (25.2 mg, 0.12 mmol) was added to the solution. The mixture was stirred at room temperature for another 12 h to give a dark green solution. Upon the addition of diethyl ether, a dark green solid was precipitated and collected. The product was recrystallized from a CH_3OH/diethyl ether mixture to afford green block-shaped crystals (**1b**). 122.72 mg, yield 87.2%. Anal. Calcd for $C_{88}H_{88}N_8O_{20}F_{12}S_4Rh_4$ (M = 2345.56): C, 45.06; H, 3.78; N, 4.78. Found: C, 45.02; H, 3.66; N,4.71. ^1H NMR (500 MHz, CD_3CN, ppm, with respect to Cp*Rh): δ = 8.56 (s, 2H, cH of -CH=N- group), δ = 8.46 (d, 4H, J=5.5 Hz, pyridyl-aH), δ = 7.80 (d, 4H, J = 5.0 Hz, pyridyl-bH), δ= 7.17 (s, 4H, phenyl-dH of E4), δ = 1.54 (s, 30H, Cp*-H).

Preparation of complex 2

AgOTf (123.2 mg, 0.48 mmol) was added to a solution of $[Cp^*RhCl_2]_2$ (37.2 mg, 0.06 mmol) in a CH_3OH (10 mL) at room temperature. The mixture was stirred in the dark for 24 h and then filtered to give a yellow solution. **L1** (25.2 mg, 0.12 mmol) was added to the filtrate. The mixture was stirred at room temperature for another 12 h to give a dark yellow solution. Upon the addition of diethyl ether, a red solid was precipitated and collected. The product was recrystallized from a CH_3OH/diethyl ether mixture to afford red block-shaped crystals (**2**). 116.13 mg, yield 86.2%. Anal. Calcd for $C_{68}H_{80}N_8O_{12}F_{12}S_4Rh_4Cl_4$ (M = 2111.10): C, 38.69; H, 3.82; N, 5.31. Found: C, 38.60; H, 3.80; N, 5.30. ^1H NMR (500 MHz, CD_3OD, ppm, with respect to Cp*Rh): δ = 8.67 (s, 2H,

cH of -CH=N- group), δ= 8.49 (d, J = 6.0Hz, 4H, pyridyl-aH), δ = 7.74 (d, J = 6.5Hz, 4H, pyridyl-bH), δ = 1.61 (s, 30H, Cp*-H).

Preparation of complex 3

AgOTf (123.2 mg, 0.48 mmol) was added to a solution of $[Cp^*RhCl_2]_2$ (74.4 mg, 0.12 mmol) in a CH_3OH (9 mL) and DMF (1mL) at room temperature. The mixture was stirred in the dark for 24 h and then filtered. $(NH_4)_2C_2O_4$ (17.0 mg, 0.12 mmol) was added to the filtrate. The mixed solution was stirred at room temperature for 12 h to give a yellow solution. **L1** (25.2 mg, 0.12 mmol) was added to the filtrate. The mixture was stirred at room temperature for another 12 h to give a yellow solution. Upon the addition of diethyl ether, a yellow solid was precipitated and collected. The product was recrystallized from a CH_3OH/diethyl ether mixture to afford yellow block-shaped crystals (**3**). 118.63 mg, yield 87.3%. Anal. Calcd for $C_{72}H_{84}N_8O_{20}F_{12}S_4Rh_4$ (M = 2149.36): C, 40.23; H, 3.94; N, 5.21. Found: C, 40.21; H, 3.90; N, 5.19. ^{1}H NMR (500 MHz, CD_3OD, ppm, with respect to Cp*Rh): δ = 8.60 (s, 2H, cH of -CH=N- group), δ = 8.22 (d, J = 6.5Hz, 4H, pyridyl-aH), δ= 7.83 (d, J = 6.5Hz, 4H, pyridyl-bH), δ = 1.62 (s, 30H, Cp*-H).

Preparation of complex 4

AgOTf (123.2 mg, 0.48 mmol) was added to a solution of $[Cp^*RhCl_2]_2$ (74.4 mg, 0.12 mmol) in a CH_3OH (9 mL) and DMSO (1 mL) at room temperature. The mixture was stirred in the dark for 24 h and then filtered. 2,5-Dihydroxy-1,4-benzoquinone (16.8 mg, 0.12 mmol) and NaOH (9.6 mg, 0.24 mmol) were added to the filtrate. The mixed solution was stirred at room temperature for 12 h to give a pale yellow solution. **L1** (25.2 mg, 0.12 mmol) was added to the filtrate. The mixture was stirred at room temperature for another 12 h to give a dark yellow solution. Upon the addition of diethyl ether, a dark yellow solid was precipitated and collected. The product was recrystallized from a CH_3OH/diethyl ether mixture to afford yellow block-shaped crystals (**4**). 114.63 mg, yield 85.20%. Anal. Calcd for $C_{80}H_{84}N_8O_{20}F_{12}S_4Rh_4$ (M = 2245.44): C, 42.79; H, 3.78; N, 4.99. Found: C, 42.71; H, 3.70; N, 4.90. ^{1}H NMR (500 MHz, CD_3OD, ppm, with respect to Cp*Rh): δ = 8.62 (s, 2H, cH of -CH=N- group), δ = 8.47 (d, J = 6.5Hz, 4H, pyridyl-aH), δ= 7.94 (d, J = 6.5Hz, 4H, pyridyl-bH), δ = 5.69 (s, 2H, phenyl-dH of E3), δ = 1.68 (s, 30H, Cp*-H).

Preparation of complex 5 ([2]catenane)

AgOTf (123.2 mg, 0.48 mmol) was added to a solution of $[Cp^*RhCl_2]_2$ (74.4 mg, 0.12 mmol) in a CH_3OH (9 mL) and DMSO (1mL) at room temperature. The mixture was stirred in the dark for 24 h and then filtered. 5,8-Dihydroxy-1,4-naphthoquinone (22.8 mg, 0.12 mmol) and NaOH (9.6 mg, 0.24 mmol) were added to the filtrate. The mixed solution was stirred at room temperature for 12 h to give a green solution. **L2** (26.9 mg, 0.12 mmol) was then added. The mixture was stirred at room temperature for another 12 h to give a dark green solution. Upon the addition of diethyl ether, a dark green solid was precipitated and collected. The product was recrystallized from a CH_3OH/diethyl ether mixture to afford green block-shaped crystals (**5**). 120.56 mg, yield 87.80%. Anal. Calcd for $C_{176}H_{168}N_{16}O_{44}F_{24}S_8Rh_8$ (M = 4747.06): C, 44.53; H, 3.57; N, 4.72. Found: C, 45.01; H, 3.70; N, 4.60. ^{1}H NMR (500 MHz, CD_3OD, ppm, with respect to Cp*Rh): δ = 8.69 (d, J = 6.5Hz, 4H, pyridyl-aH), δ = 8.13 (d, J = 6.5Hz, 4H, pyridyl-bH), δ= 7.24 (s, 4H, phenyl-cH of E4), δ = 1.62 (s, 30, Cp*-H).

Preparation of complex 6

AgOTf (123.2 mg, 0.48 mmol) was added to a solution of $[Cp^*RhCl_2]_2$ (74.4 mg, 0.12 mmol) in a CH_3OH (10 mL) at room temperature. The mixture was stirred in the dark for 24 h and then filtered. 2,5-Dihydroxy-1,4-benzoquinone (16.8 mg, 0.12 mmol) and NaOH (9.6 mg, 0.24 mmol) were added to the filtrate. The mixed solution was stirred at room temperature for 12 h to give a brown solution. **L2** (26.9 mg, 0.12 mmol) was then added. The mixture was stirred at room temperature for another 12 h to give a dark brown solution. Upon the

addition of diethyl ether, a dark brown solid was precipitated and collected. The product was recrystallized from a CH_3OH/diethyl ether mixture to afford brown block-shaped crystals (**6**). 120.56 mg, yield 87.80%. Anal. Calcd for $C_{80}H_{80}N_8O_{22}F_{12}S_4Rh_4$ (M = 2273.41): C, 42.27; H, 3.55; N, 4.93. Found: C, 42.21; H, 3.52; N, 4.90. ^{1}H NMR (500 MHz, CD_3OD, ppm, with respect to Cp*Rh): δ = 8.61 (d, J = 6.5Hz, 4H, pyridyl-aH), δ = 8.21 (d, J = 6.5Hz, 4H, pyridyl-bH), δ= 5.70 (s, 2H, phenyl-cH of E3), δ = 1.69 (s, 30H, Cp*-H).

Preparation of complex 7

AgOTf (123.2 mg, 0.48 mmol) was added to a solution of $[Cp^*RhCl_2]_2$ (74.4 mg, 0.12 mmol) in a CH_3OH (10 mL) at room temperature. The mixture was stirred in the dark for 24 h and then filtered. 6,11-Dihydroxy-5,12-naphthacenedione (34.8 mg, 0.12 mmol) and NaOH (9.6 mg, 0.24 mmol) were added to the filtrate. The mixed solution was stirred at room temperature for 12 h to give a blue-black solution. **L2** (26.9 mg, 0.12 mmol) was then added. The mixture was stirred at room temperature for another 12 h to give a blue-black solution. Upon the addition of diethyl ether, a blue-black solid was precipitated and collected. The product was recrystallized from a CH_3OH/diethyl ether mixture to afford blue-black block-shaped crystals (**7**). 120.23 mg, yield 87.42%. Anal. Calcd for $C_{104}H_{92}N_8O_{22}F_{12}S_4Rh_4$ (M = 2573.77): C, 48.53; H, 3.60; N, 4.35. Found: C, 48.28; H, 3.54; N, 4.30. ^{1}H NMR (500 MHz, CD_3OD, ppm, with respect to Cp*Rh): δ = 8.77 (d, 4H, J = 5.0Hz, pyridyl-aH), δ = 8.77-8.76 (d, 4H, phenyl-cH of E5), δ= 8.00 (d, J = 5.5Hz, 4H, pyridyl-bH), δ = 7.97-7.95 (m, 4H, phenyl-dH of E5), δ = 1.73 (s, 30H, Cp*-H).

3. NMR Spectra

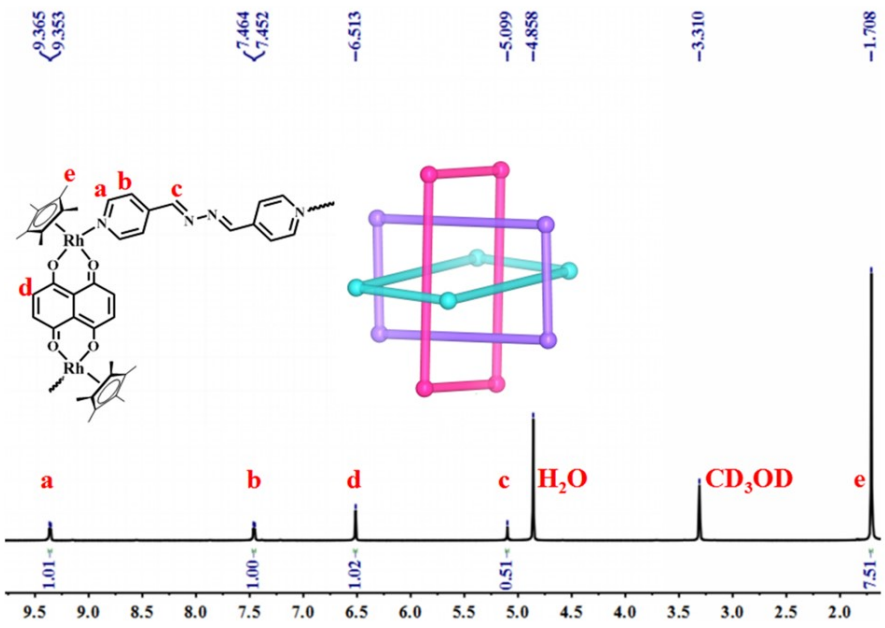

Figure S1. The ^{1}H NMR (500 MHz, CD_3OD, ppm) for Borromean ring **1a** (16.0 mM, with respect to Cp*Rh).

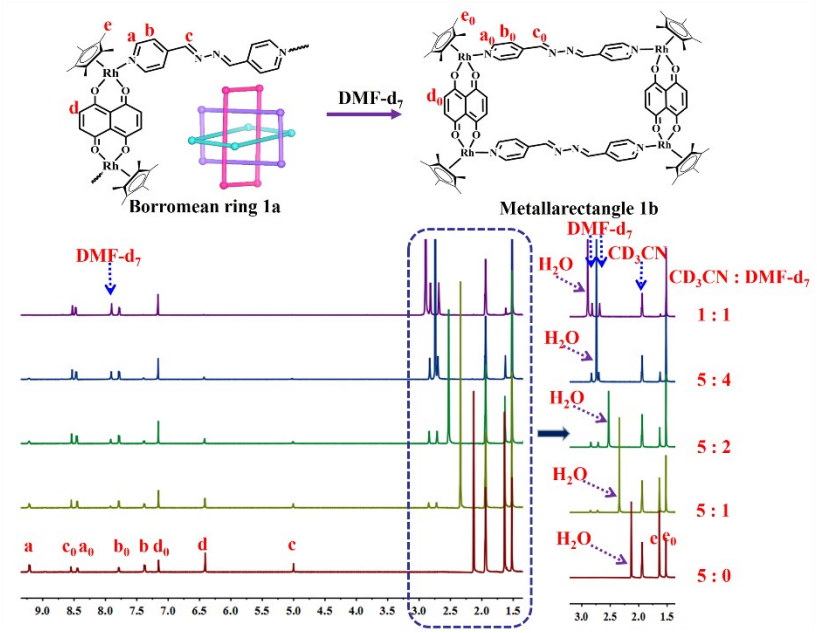

Figure S2. The full ^{1}H NMR spectra showing the interconversion from the mixture of Borromean ring **1a** and tetranuclear macrocycle **1b** to complex **1b** upon changing solvent ratio (CD_3CN/DMF-d_7 [18.0 mM, with respect to Cp*Rh], 500 MHz).

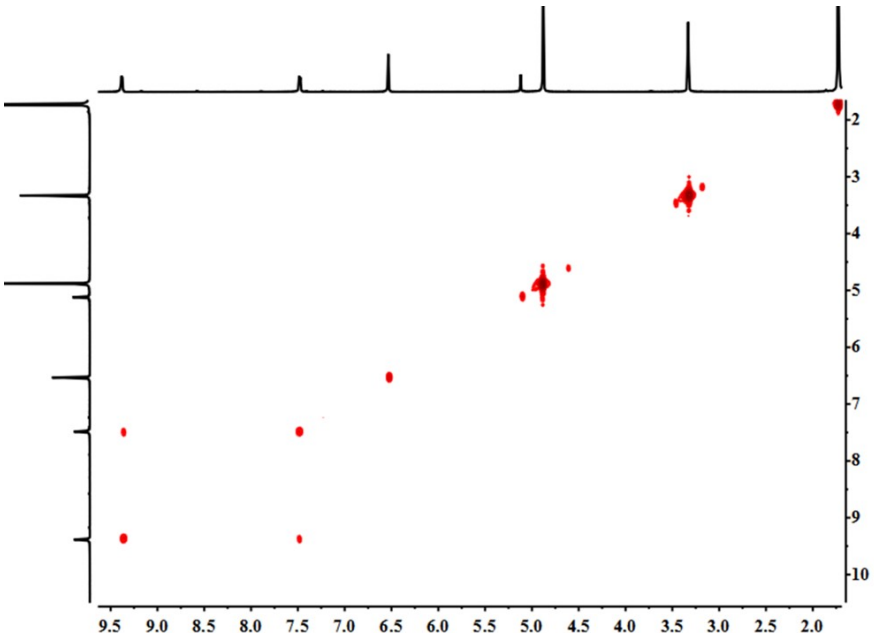

Figure S3. The ^{1}H-^{1}H COSY NMR (500 MHz, CD_3OD, ppm) for Borromean ring **1a** (16.0 mM, with respect to Cp*Rh).

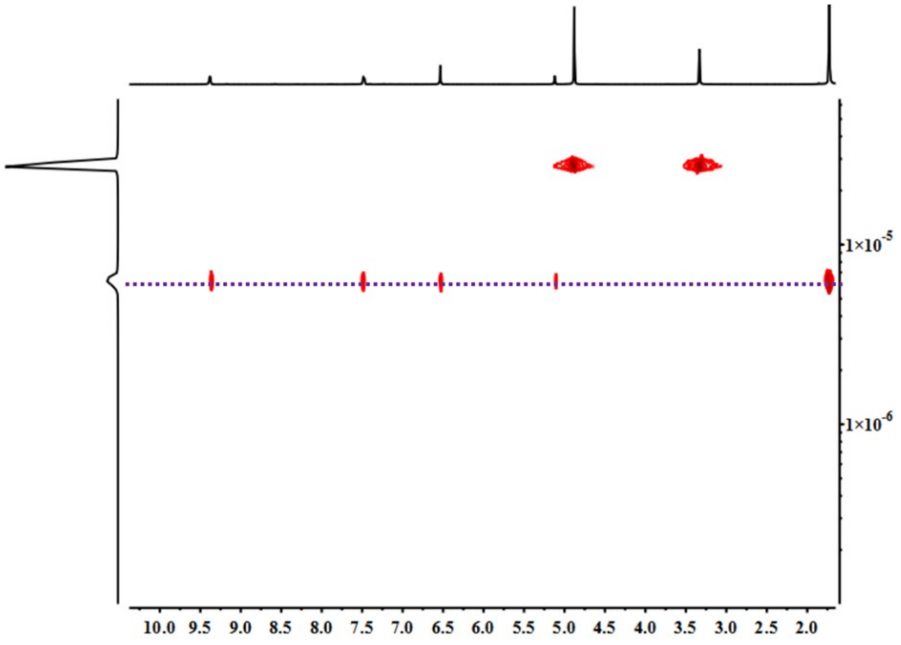

Figure S4. The ^{1}H-^{1}H DOSY NMR (500 MHz, CD_3OD, ppm) for Borromean ring **1a** (2.57×10^{-10} m^2s^{-1}) (16.0 mM, with respect to Cp*Rh).

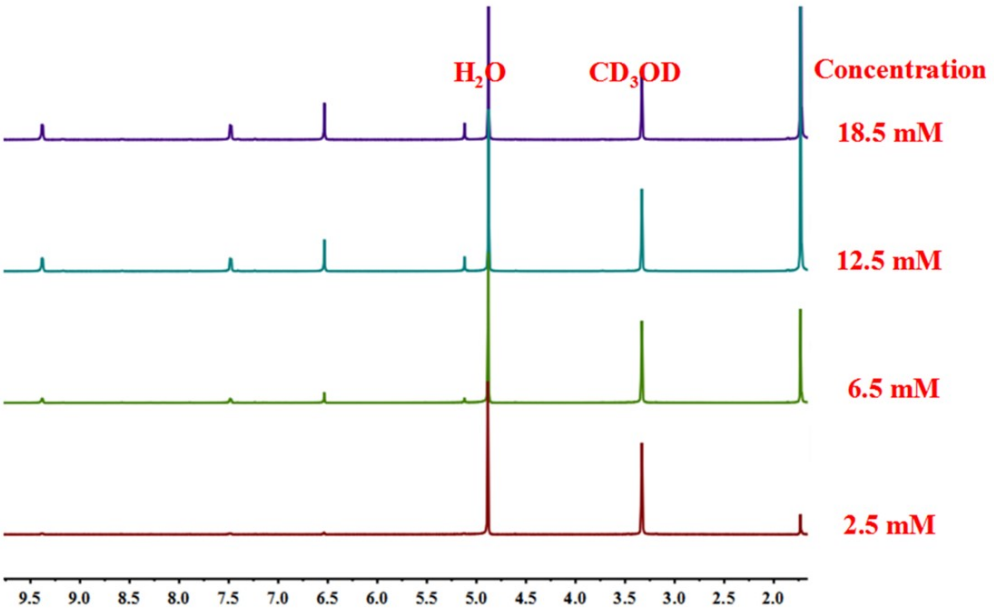

Figure S5. The ^{1}H NMR (500 MHz, CD_3OD, ppm) for Borromean ring **1a**, showing high concentration stability of Borromean ring **1a** in a methanol solution**.** (2.5-18.5 mM, with respect to Cp*Rh).

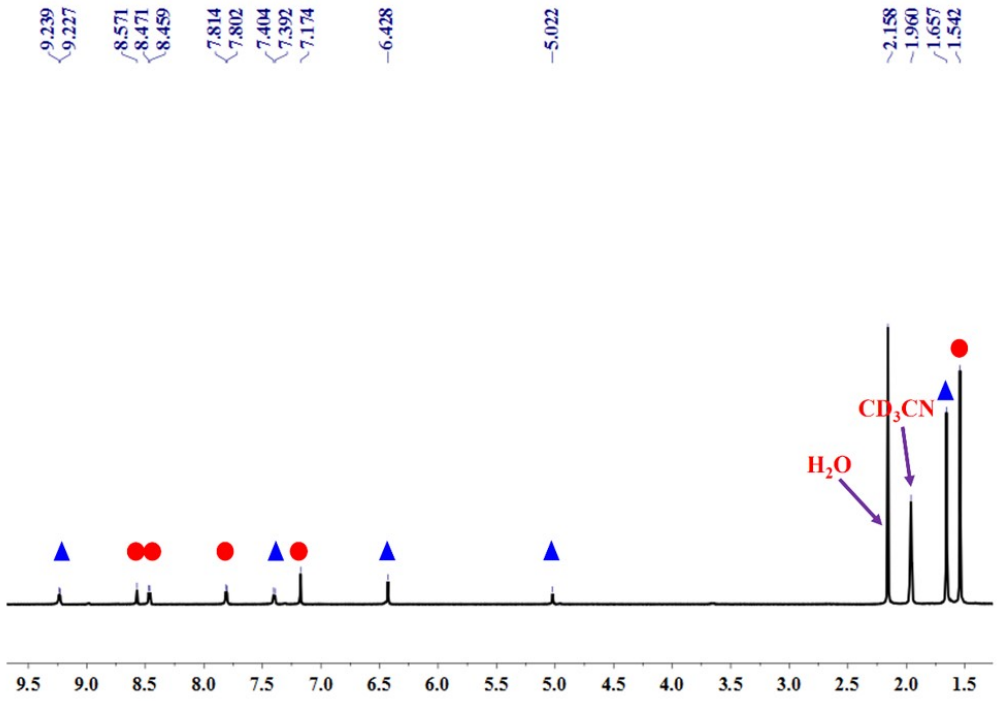

Figure S6. ^{1}H NMR (400 MHz, CD_3CN, ppm) for **1a** + **1b** (16.0mM, Blue triangle for **1a**, Red circle for **1b**).

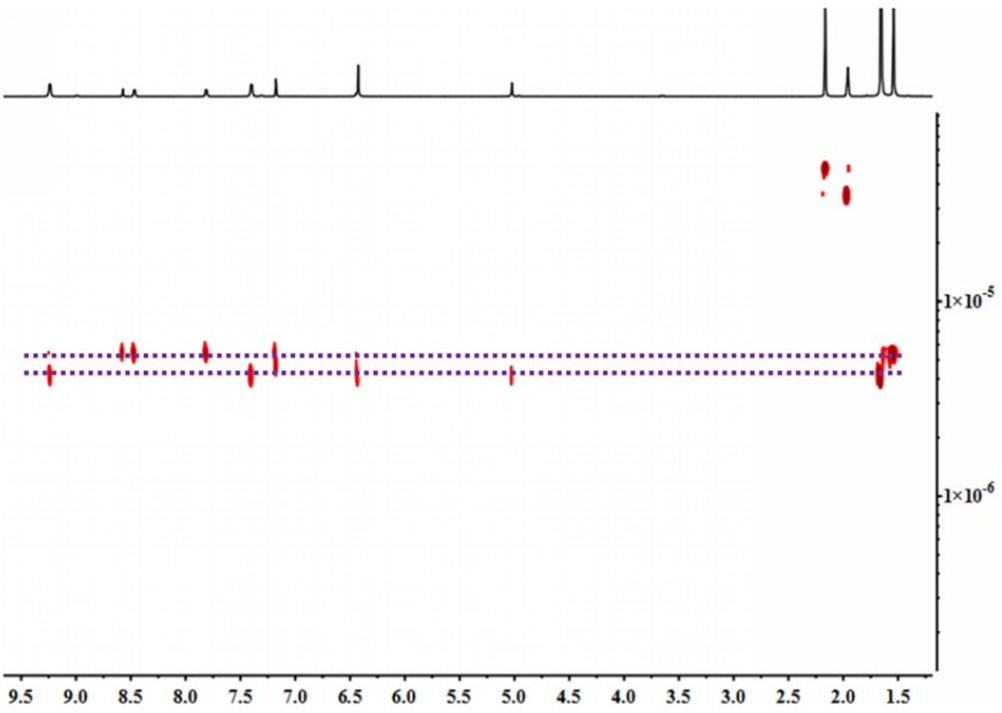

Figure S7. ^{1}H DOSY NMR (500 MHz, CD_3CN, ppm) for **1a**+**1b** (16.0 mM, with respect to Cp*Rh). This DOSY spectra showed that Borromean ring **1a** and metallarectangle **1b** existed at the same time in a medium-concentration solution Diffusion coefficient for **1a**: 5.37×10^{-10} m^2s^{-1} and **1b**: 3.90×10^{-10} m^2s^{-1}.

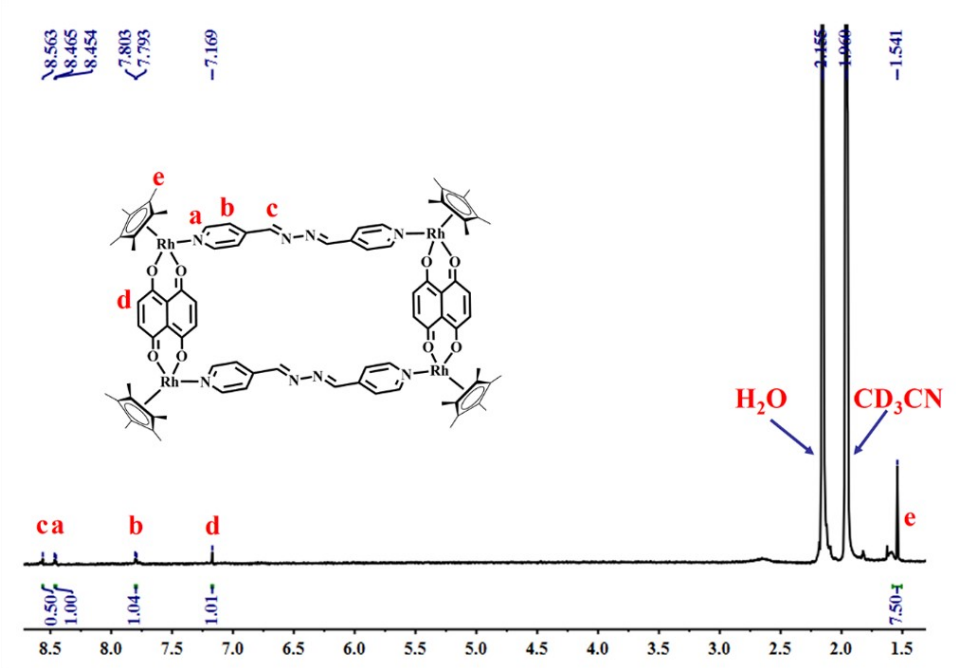

Figure S8. The ^{1}H NMR (500 MHz, CD_3CN, ppm) for metallarectangle **1b** (1.0 mM, with respect to Cp*Rh).

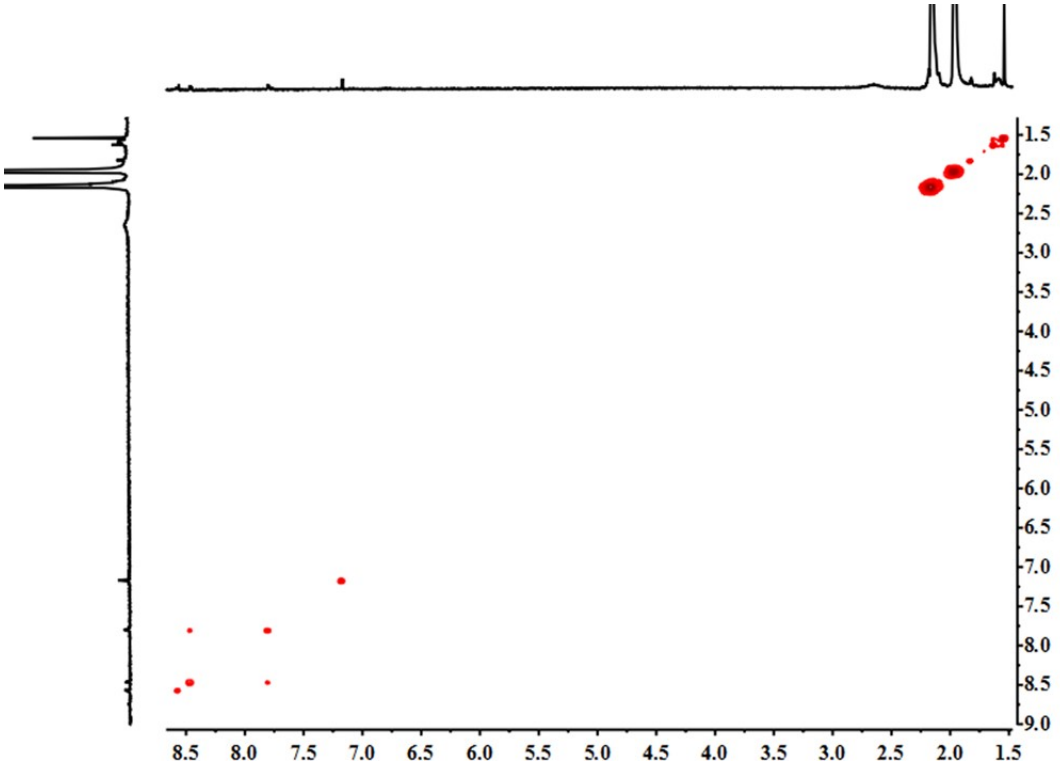

Figure S9. The ^{1}H-^{1}H COSY NMR (500 MHz, CD_3CN, ppm) for metallarectangle **1b** (1.0 mM, with respect to Cp*Rh).

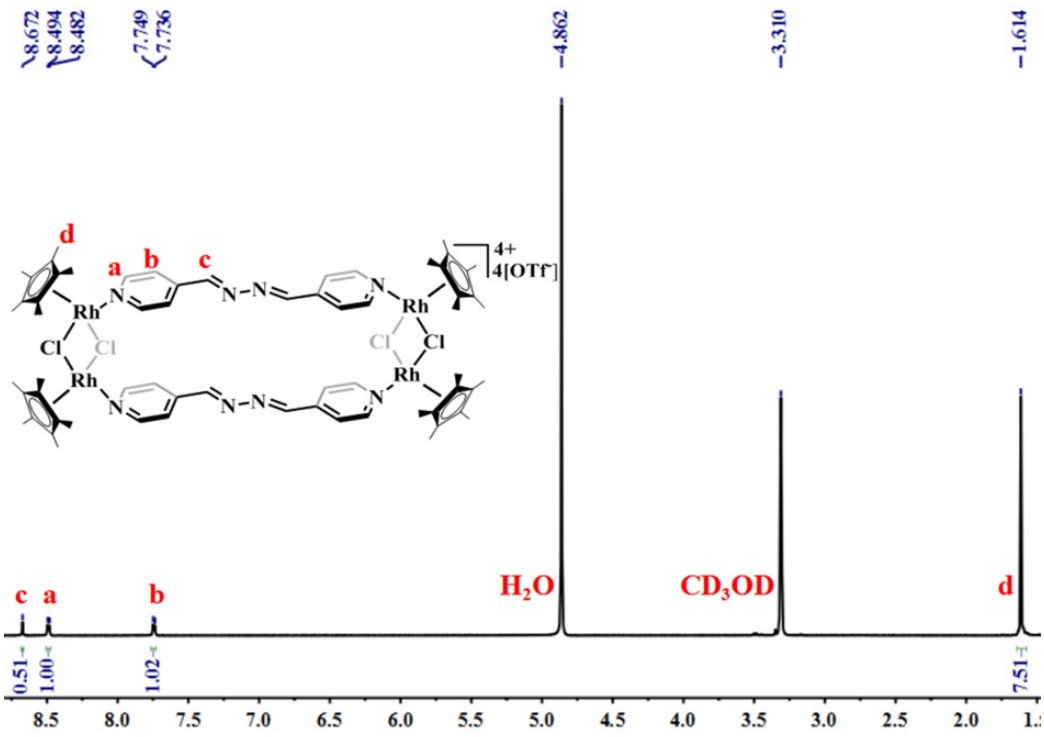

Figure S10. The ^{1}H NMR (500 MHz, CD_3OD, ppm) for metallarectangle **2** (8.0 mM, with respect to Cp*Rh).

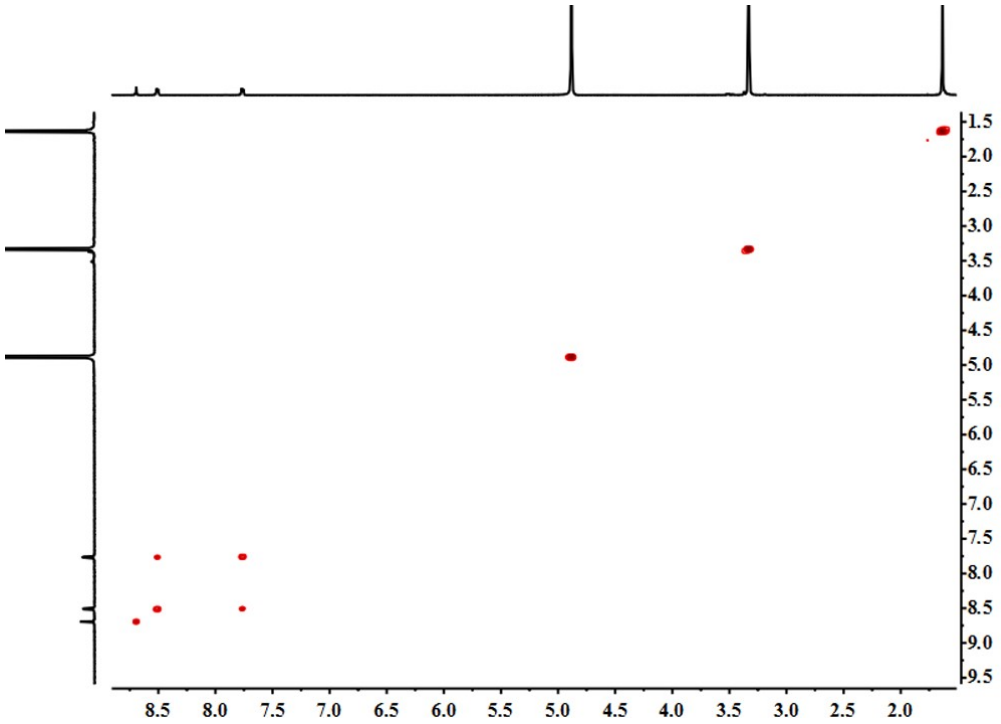

Figure S11. The ^{1}H-^{1}H COSY NMR (500 MHz, CD_3OD, ppm) for metallarectangle **2** (8.0 mM, with respect to Cp*Rh).

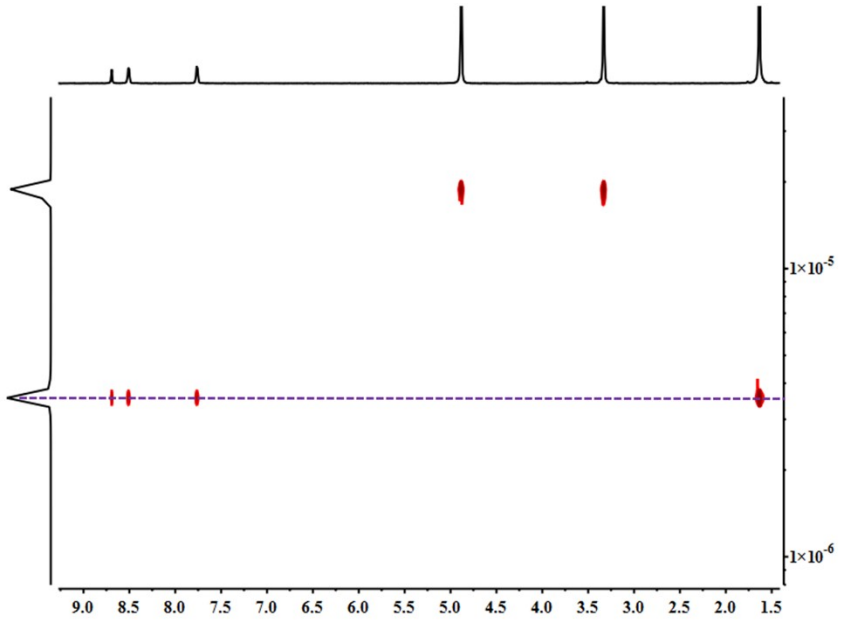

Figure S12. The ^{1}H-^{1}H DOSY NMR (500 MHz, CD_3OD, ppm) for metallarectangle **2** ($D = 3.53 \times 10^{-10}$ m^2s^{-1}) (10.0 mM, with respect to Cp*Rh).

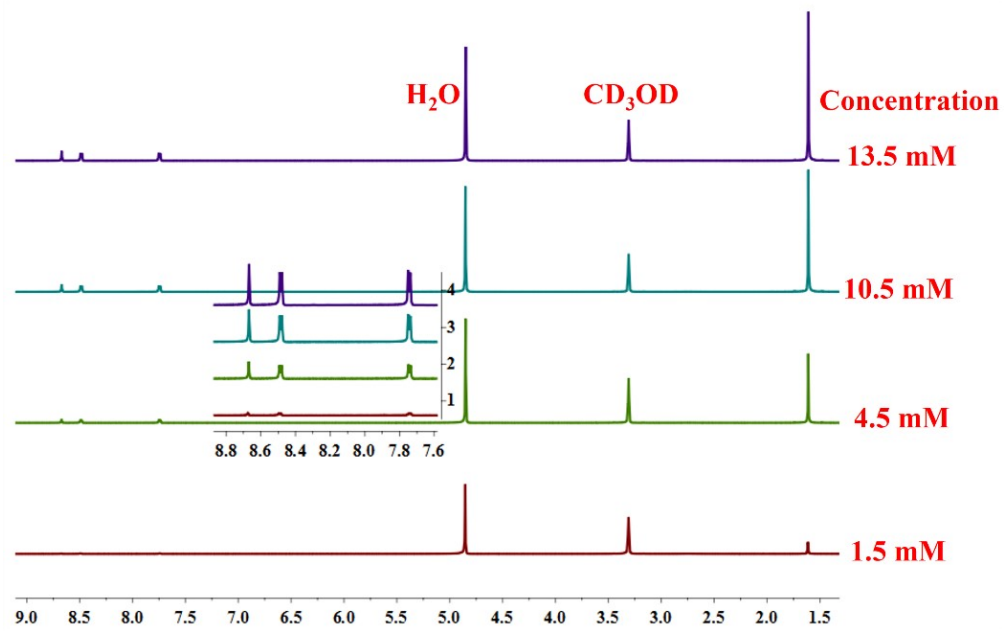

Figure S13. The ^{1}H NMR (500 MHz, CD_3OD, ppm) for tetranuclear complex **2**, showing high concentration stability of **2** in a methanol solution**.** (1.5-13.5 mM, with respect to Cp*Rh).

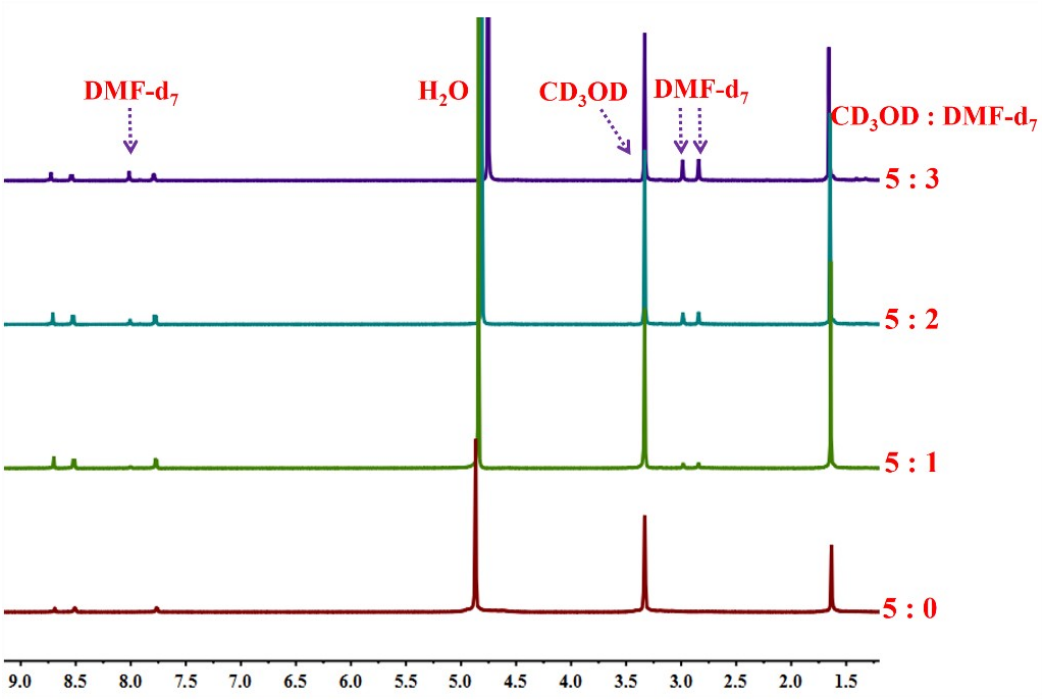

Figure S14. The full ^{1}H NMR spectra showing no interconversion between tetranuclear complex **2** and other complex upon changing solvent ratio (CD_3OD/DMF-d_7 [15.0 mM, with respect to Cp*Rh], 500 MHz).

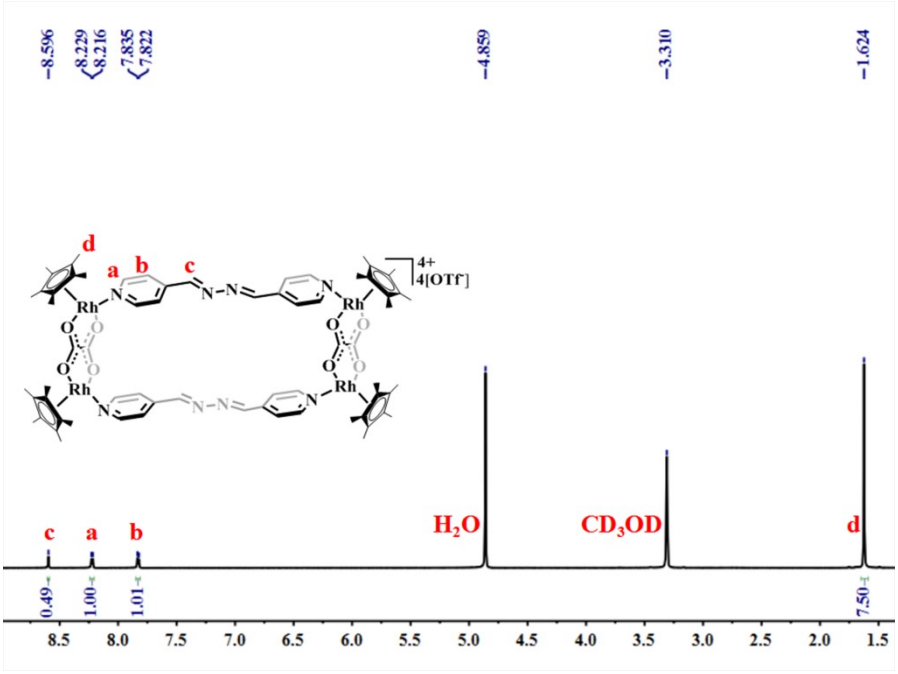

Figure S15. The ^{1}H NMR (500 MHz, CD_3OD, ppm) for metallarectangle **3** (18.0 mM, with respect to Cp*Rh).

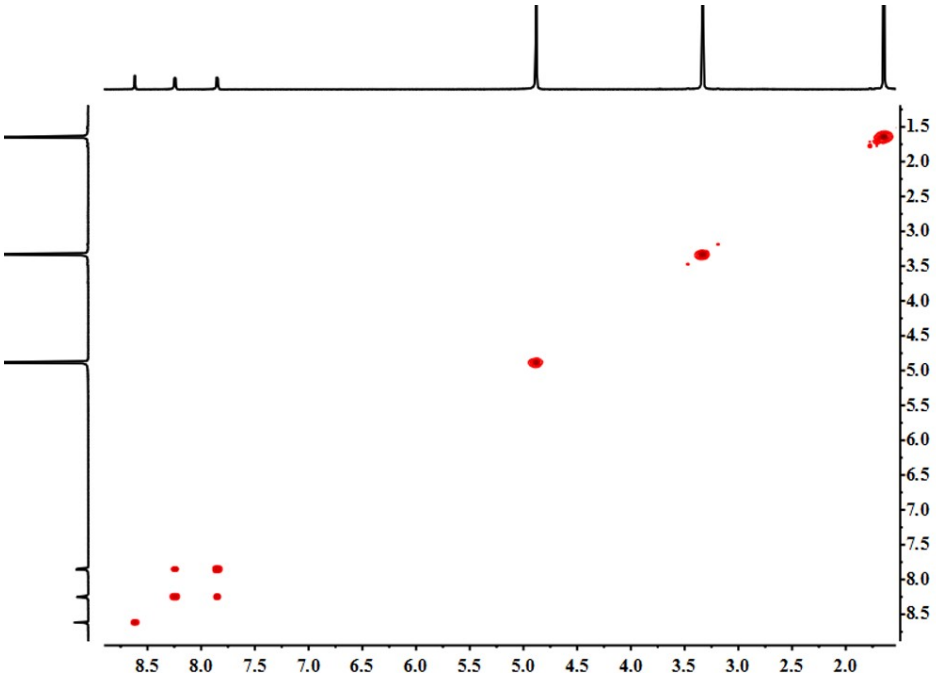

Figure S16. The ^{1}H-^{1}H COSY NMR (500 MHz, CD_3OD, ppm) for metallarectangle **3** (18.0 mM, with respect to Cp*Rh).

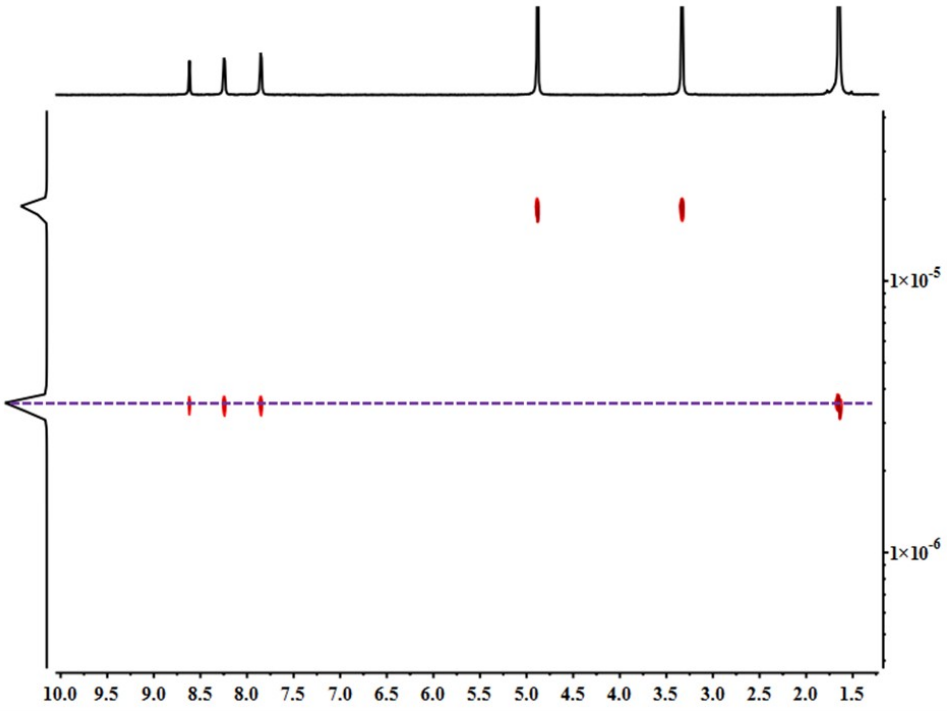

Figure S17. The ^{1}H-^{1}H DOSY NMR (500 MHz, CD_3OD, ppm) for metallarectangle **3** ($D = 3.45 \times 10^{-10}$ m^2s^{-1}) (18.0 mM, with respect to Cp*Rh).

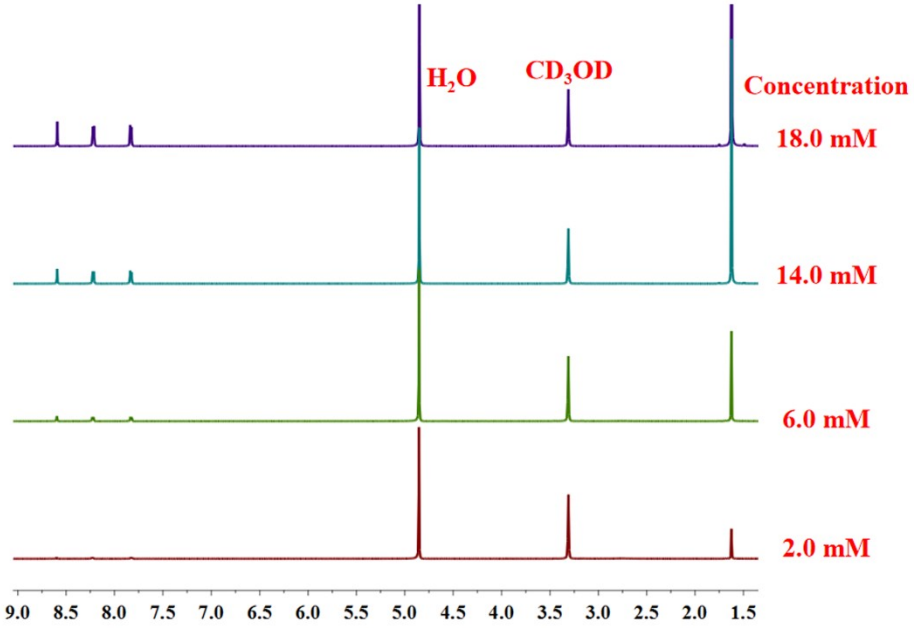

Figure S18. The ^{1}H NMR (500 MHz, CD_3OD, ppm) for tetranuclear complex **3**, showing high concentration stability of **3** in a methanol solution**.** (2.0-18.0 mM, with respect to Cp*Rh).

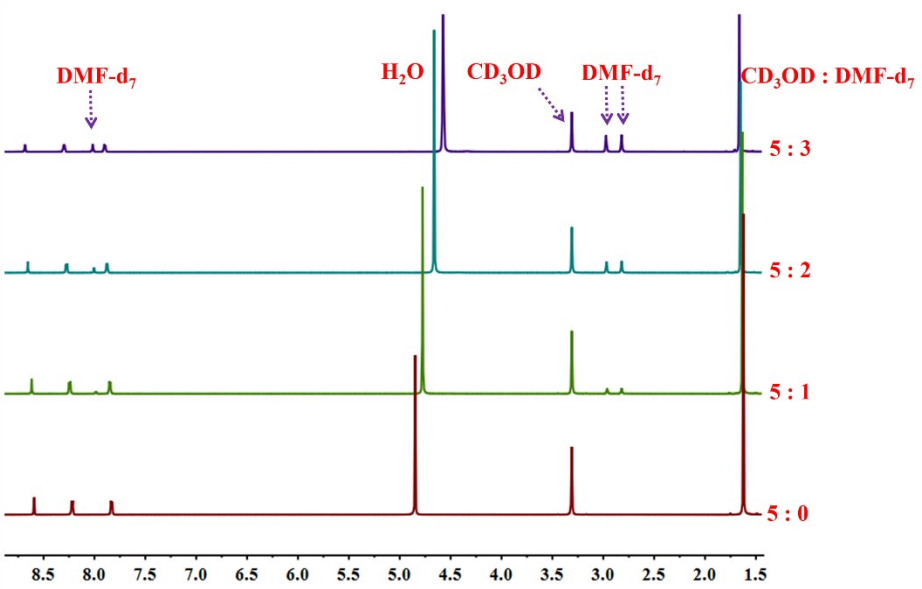

Figure S19. The full ^{1}H NMR spectra showing no interconversion between tetranuclear complex **3** and other complex upon changing solvent ratio (CD_3OD/DMF-d_7 [25.0 mM, with respect to Cp*Rh], 500 MHz).

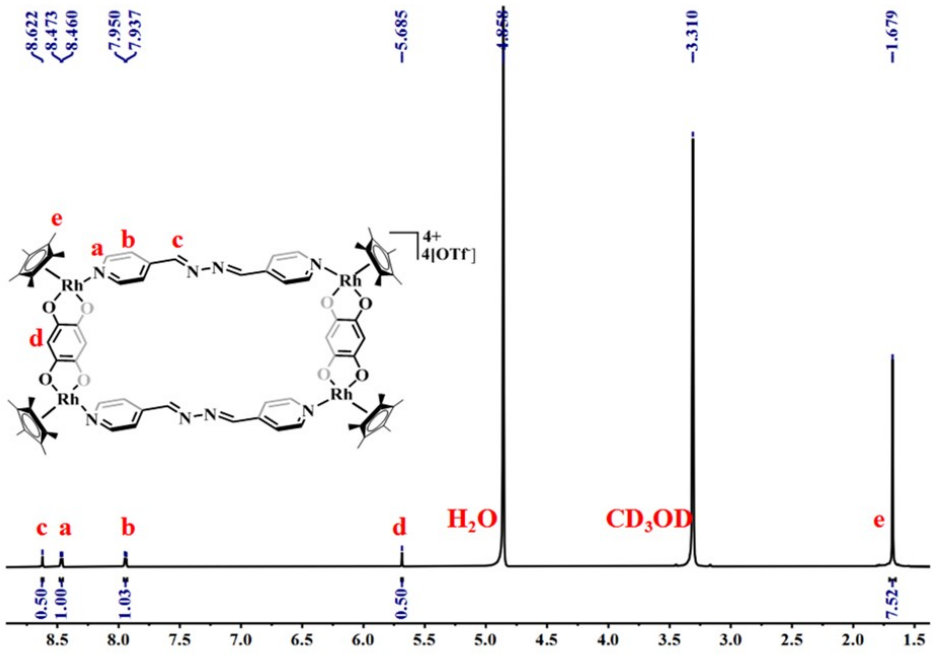

Figure S20. The ^{1}H NMR (500 MHz, CD_3OD, ppm) for metallarectangle **4** (10.0 mM, with respect to Cp*Rh).

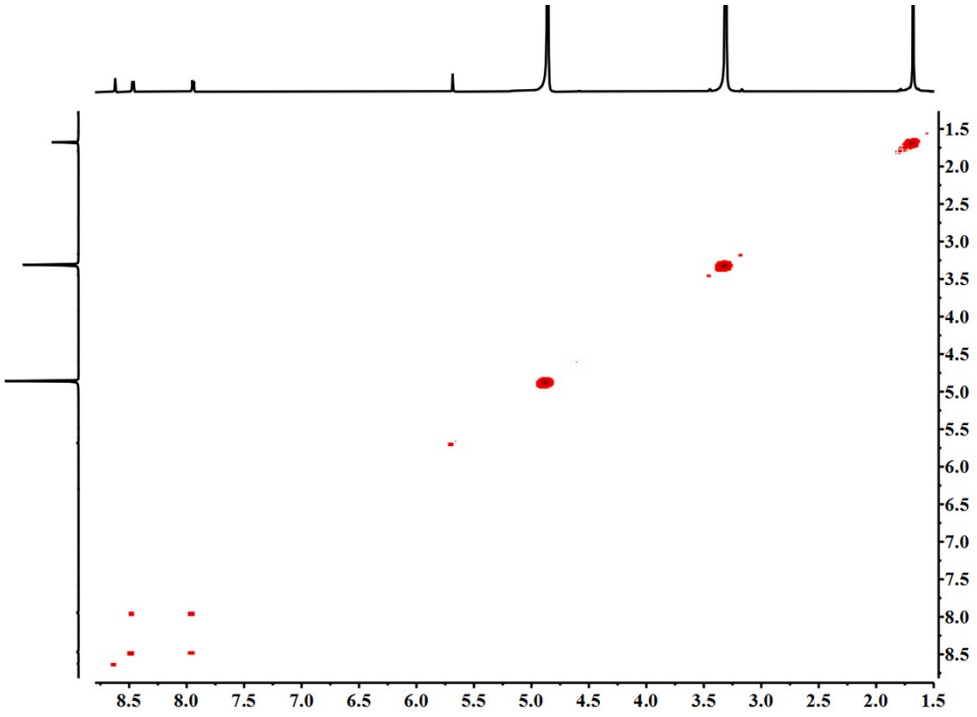

Figure S21. The ^{1}H-^{1}H COSY NMR (500 MHz, CD_3OD, ppm) for metallarectangle **4** (10.0 mM, with respect to Cp*Rh).

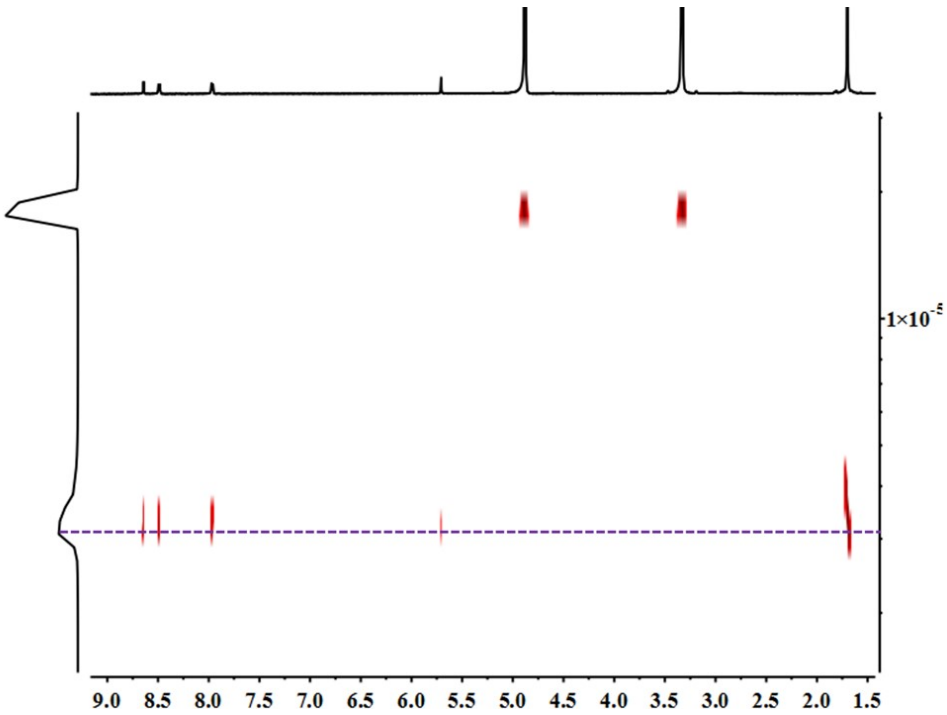

Figure S22. The ^{1}H-^{1}H DOSY NMR (500 MHz, CD_3OD, ppm) for metallarectangle **4** ($D = 3.32 \times 10^{-10}$ m^2s^{-1}) (10.0 mM, with respect to Cp*Rh).

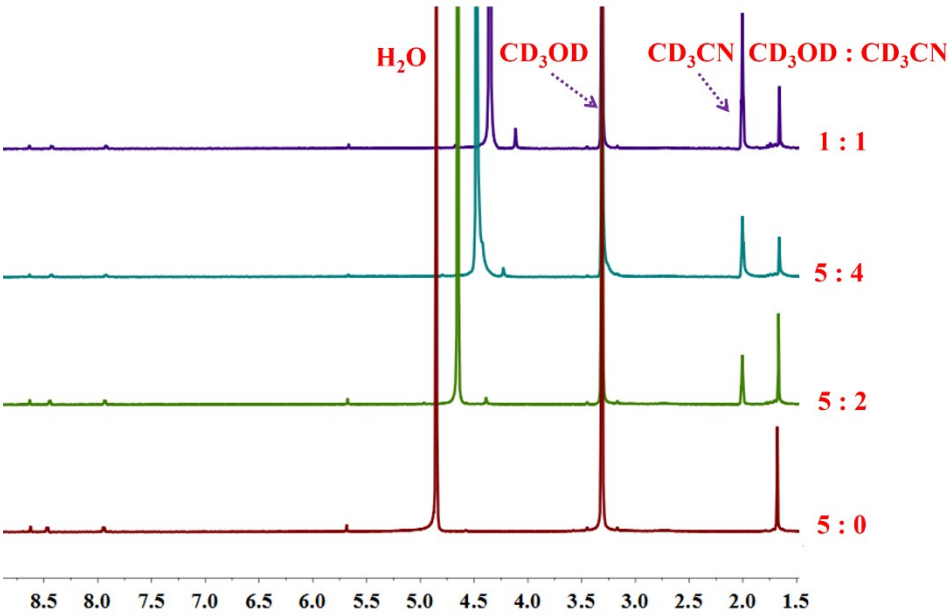

Figure S23. The full ^{1}H NMR spectra showing no interconversion between tetranuclear complex **4** and other complex upon changing solvent ratio (CD_3OD/CD_3CN [10.0 mM, with respect to Cp*Rh], 500 MHz).

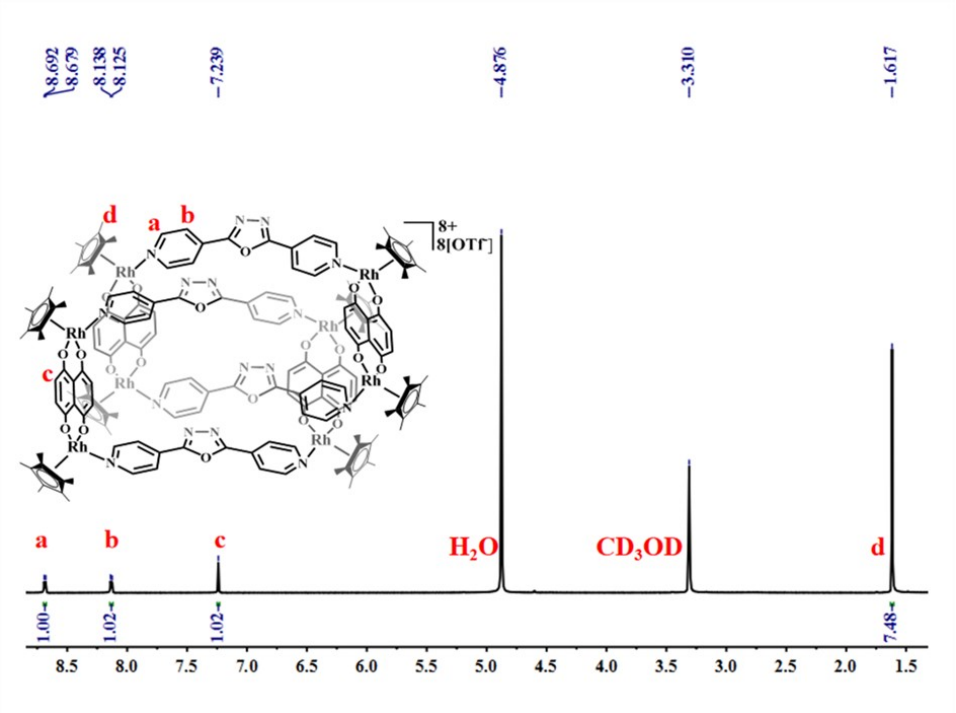

Figure S24. The ^{1}H NMR (500 MHz, CD_3OD, ppm) for [2]catenane **5** (10.0 mM, with respect to Cp*Rh).

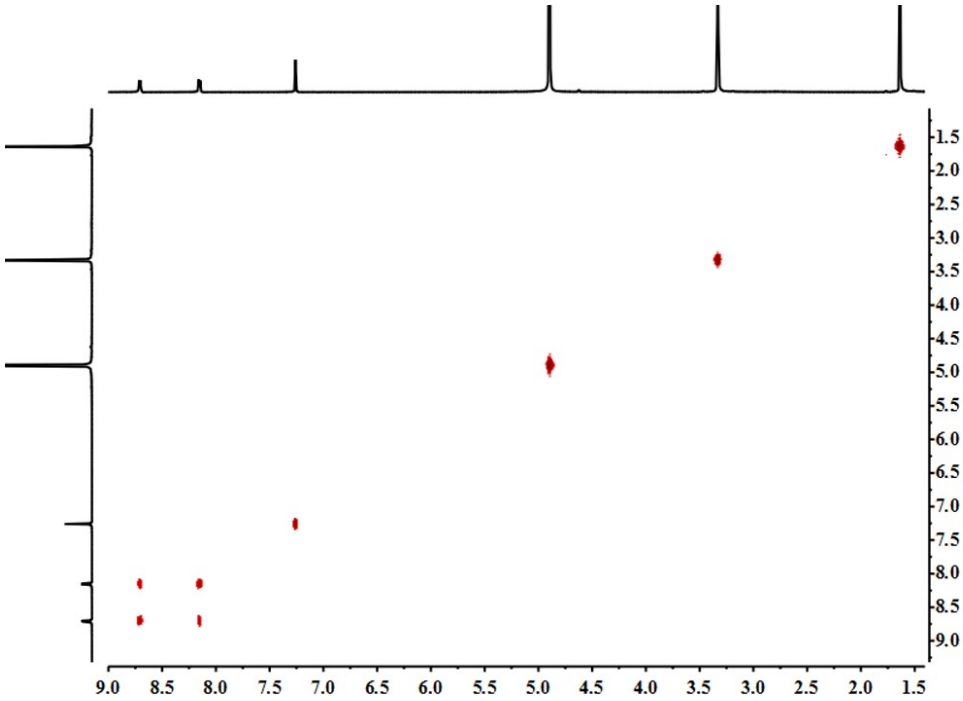

Figure S25. The ^{1}H-^{1}H COSY NMR (500 MHz, CD_3OD, ppm) for [2]catenane **5** (10.0 mM, with respect to Cp*Rh).

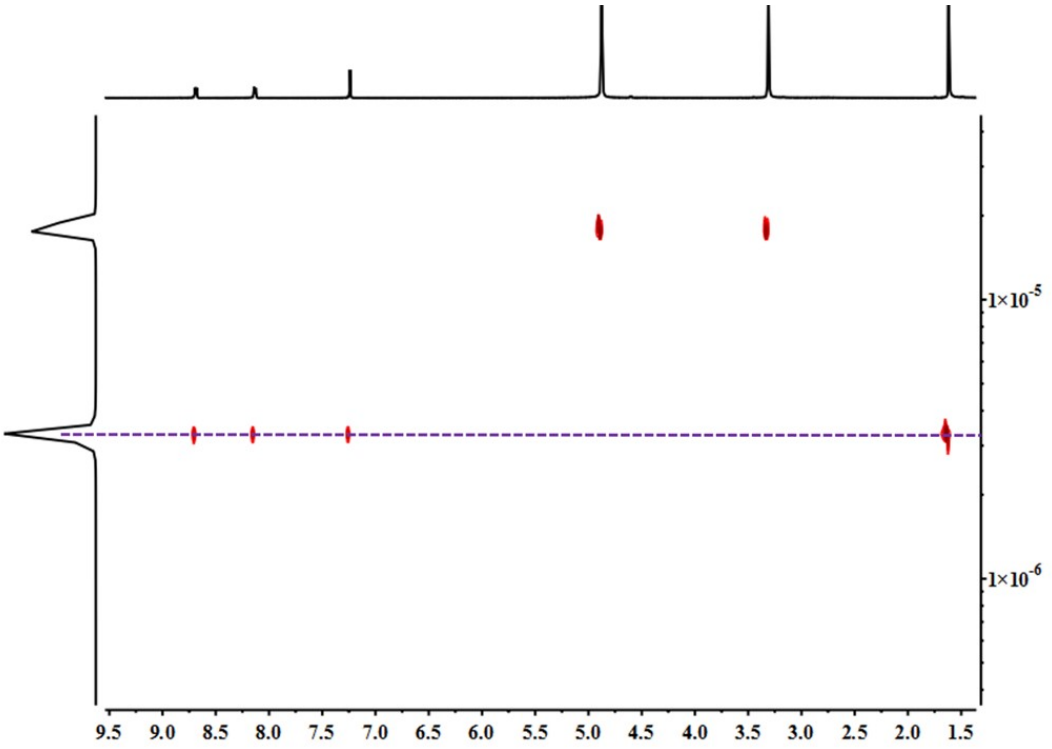

Figure S26. The ^{1}H-^{1}H DOSY NMR (500 MHz, CD_3OD, ppm) for [2]catenane **5** ($D = 3.22 \times 10^{-10}$ m^2s^{-1}) (10.0 mM, with respect to Cp*Rh).

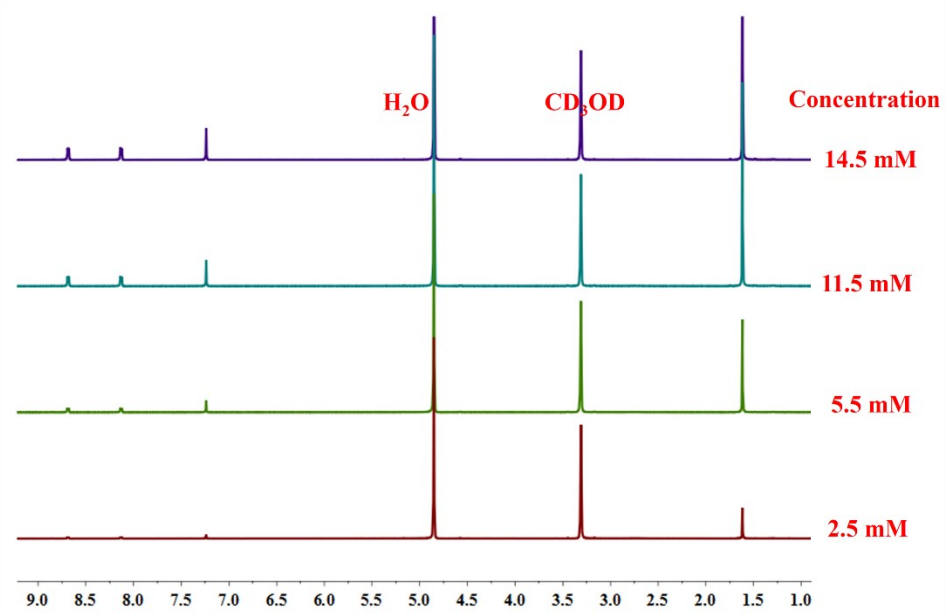

Figure S27. The ^{1}H NMR (500 MHz, CD_3OD, ppm) for [2] catenane **5**, showing high concentration stability of [2] catenane **5** in a methanol solution**.** (2.5-14.5 mM, with respect to Cp*Rh).

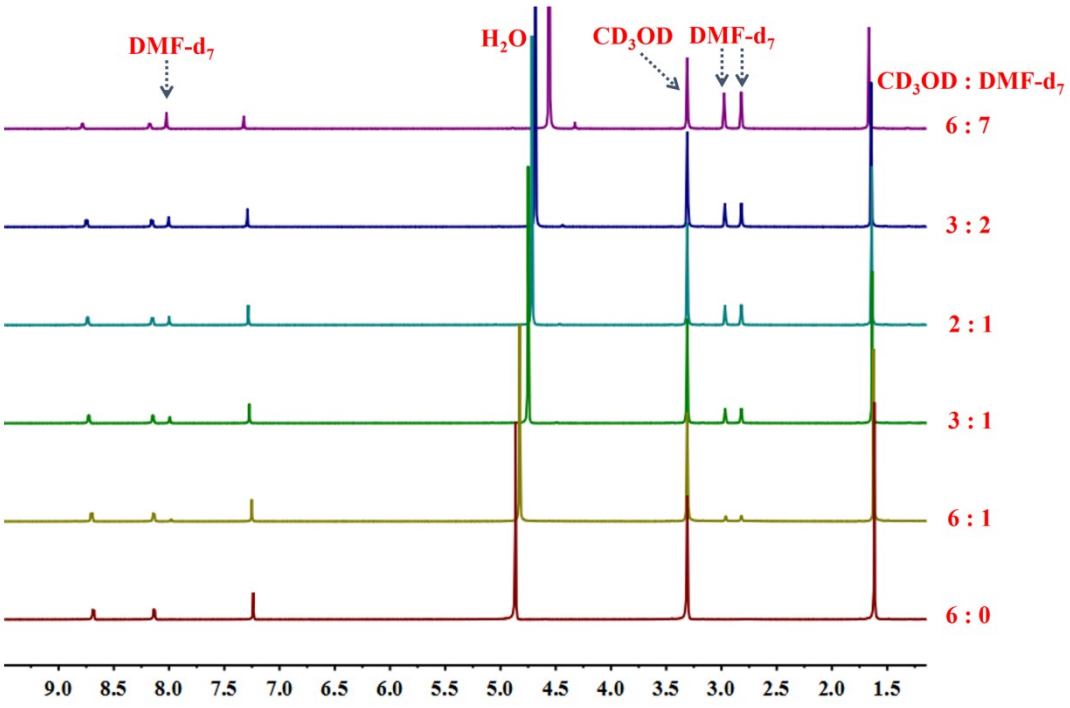

Figure S28. The full ^{1}H NMR spectra showing no interconversion between [2] catenane **5** and other complex upon changing solvent ratio (CD_3OD/DMF-d_7 [15.0 mM, with respect to Cp*Rh], 500 MHz).

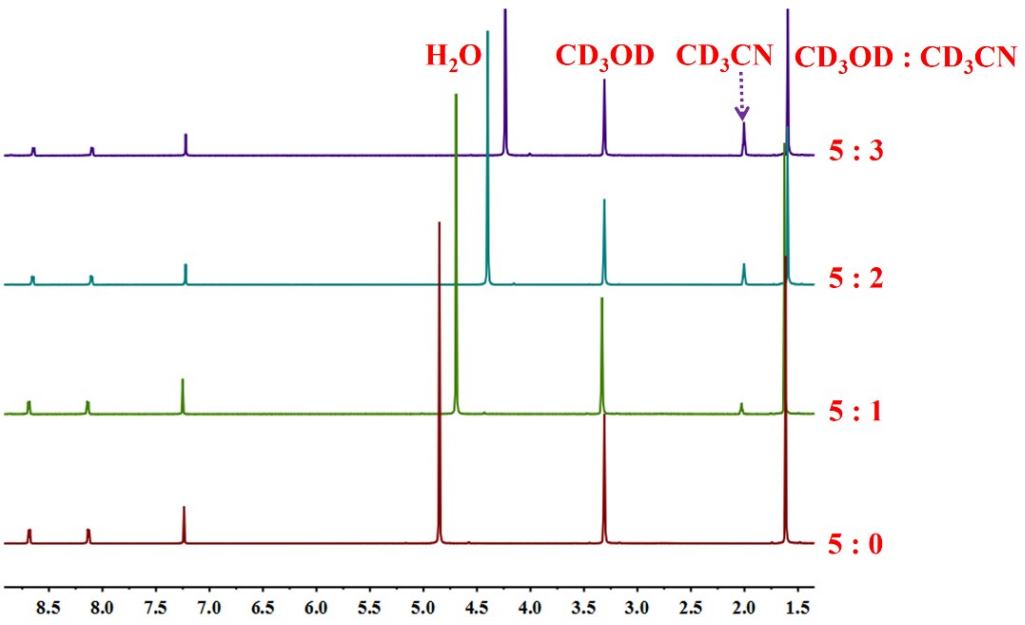

Figure S29. The full ^{1}H NMR spectra showing no interconversion between [2] catenane **5** and other complex upon changing solvent ratio (CD_3OD/CD_3CN [20.0 mM, with respect to Cp*Rh], 500 MHz).

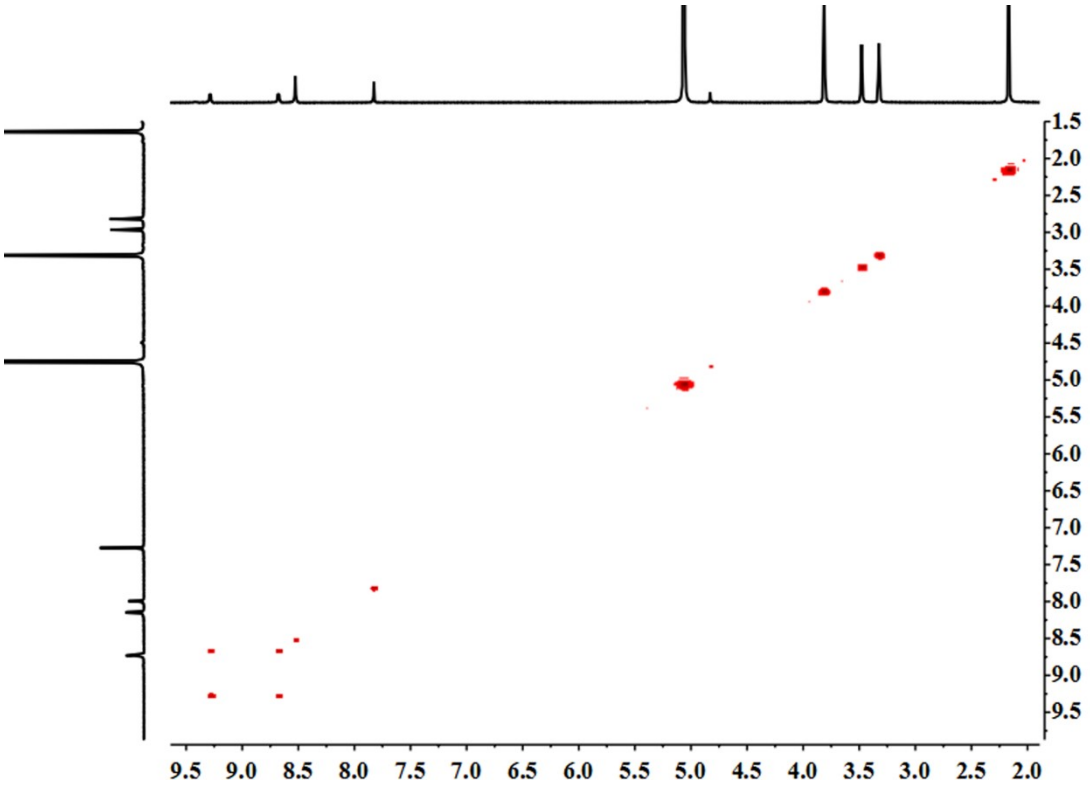

Figure S30. The ^{1}H-^{1}H COSY NMR (500 MHz, CD_3OD, ppm) for [2]catenane **5** under the condition of solvent ratio (CD_3OD/DMF-d_7 = 6 : 7 [15.0 mM, with respect to Cp*Rh], 500 MHz).

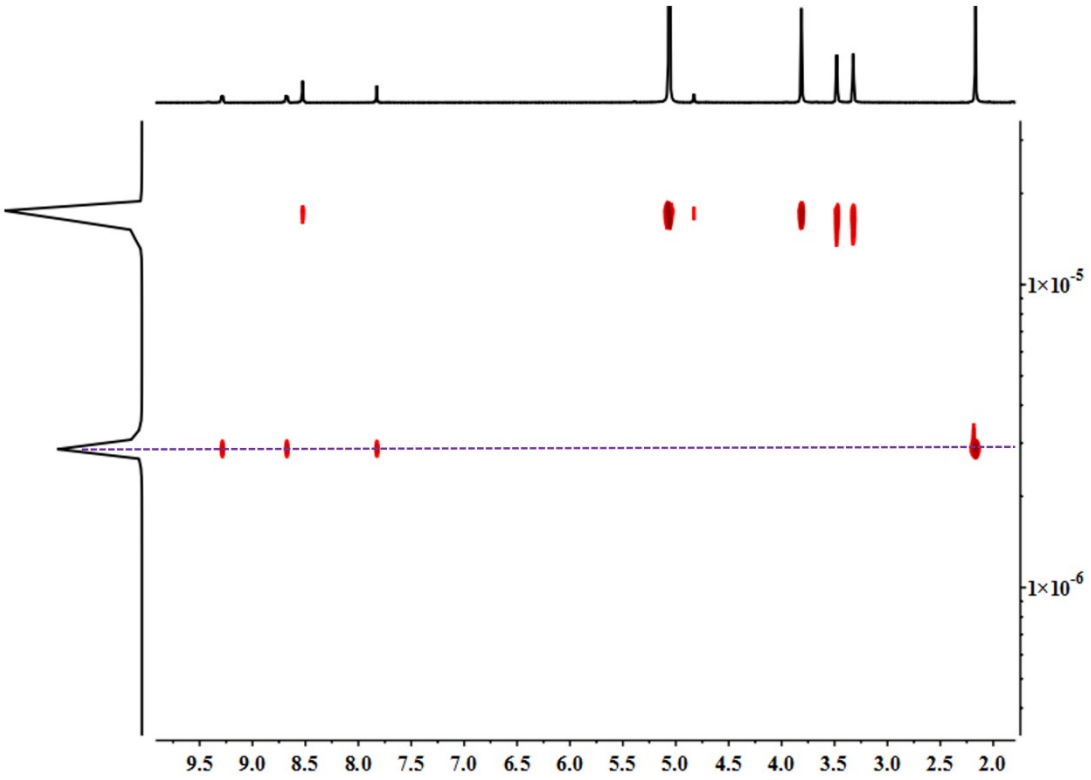

Figure S31. The ^{1}H-^{1}H DOSY NMR (500 MHz, CD_3OD, ppm) for [2]catenane **5** under the condition of solvent ratio (CD_3OD/DMF-d_7 = 6 : 7 [D = 2.88 × 10^{-10} m^2s^{-1}, 15.0 mM, with respect to Cp*Rh], 500 MHz).

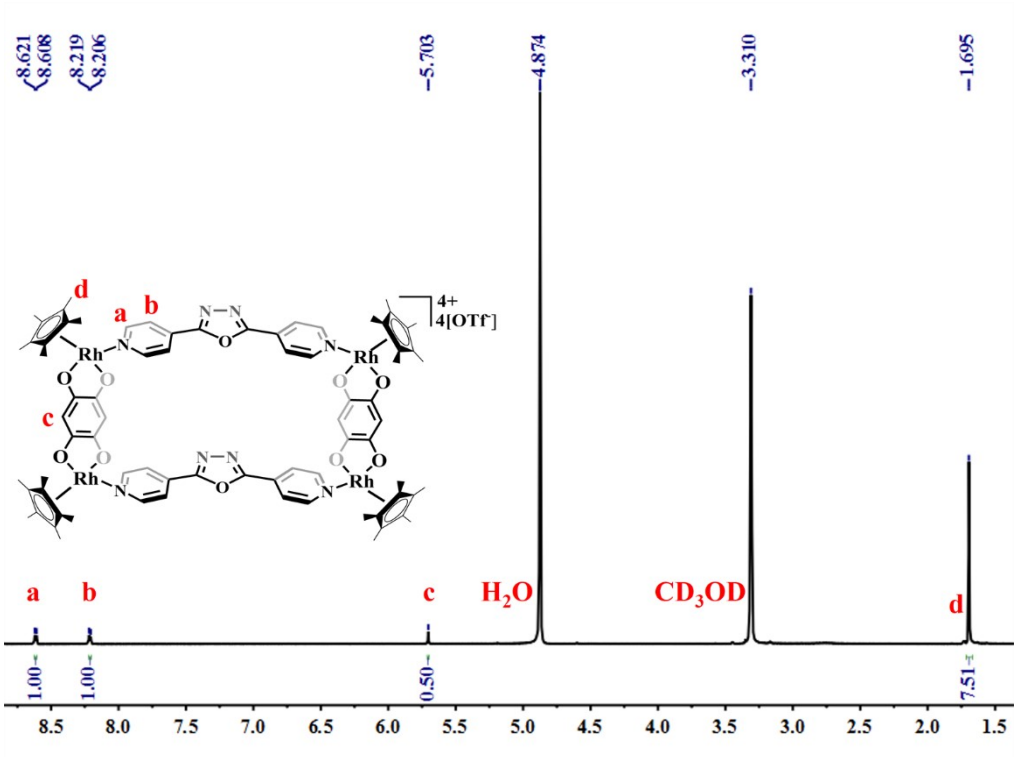

Figure S32. The ^{1}H NMR (500 MHz, CD_3OD, ppm) for metallarectangle **6** (9.0 mM, with respect to Cp*Rh).

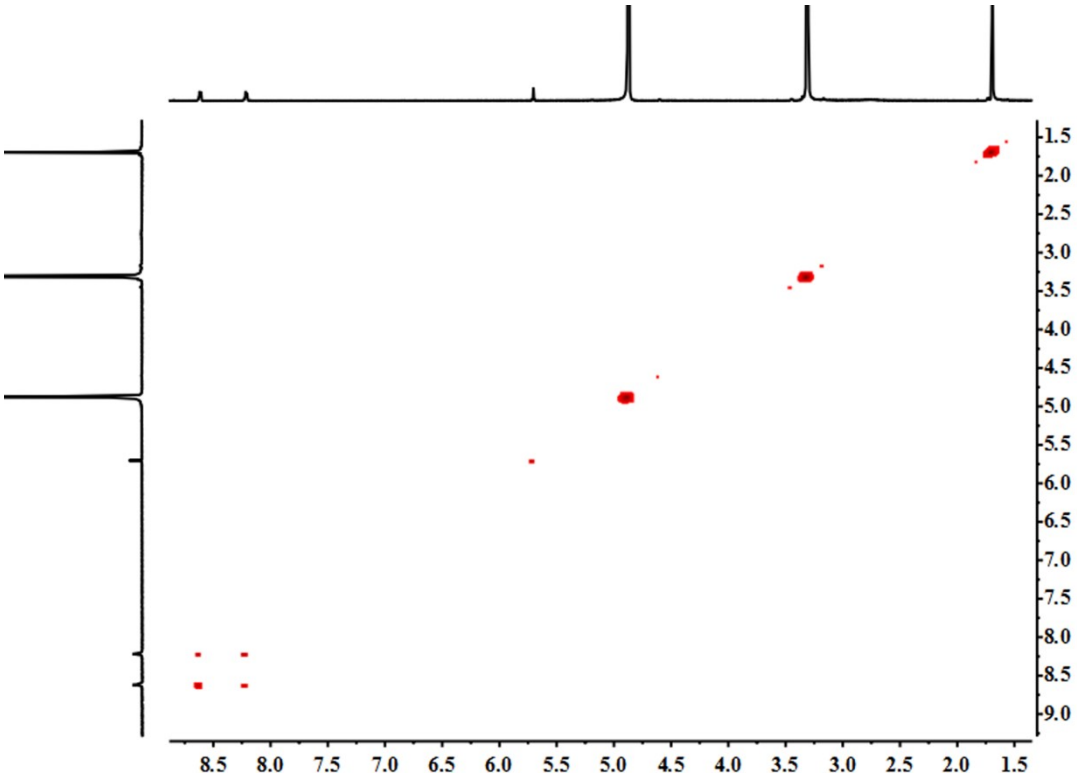

Figure S33. The ^{1}H-^{1}H COSY NMR (500 MHz, CD_3OD, ppm) for metallarectangle **6** (9.0 mM, with respect to Cp*Rh).

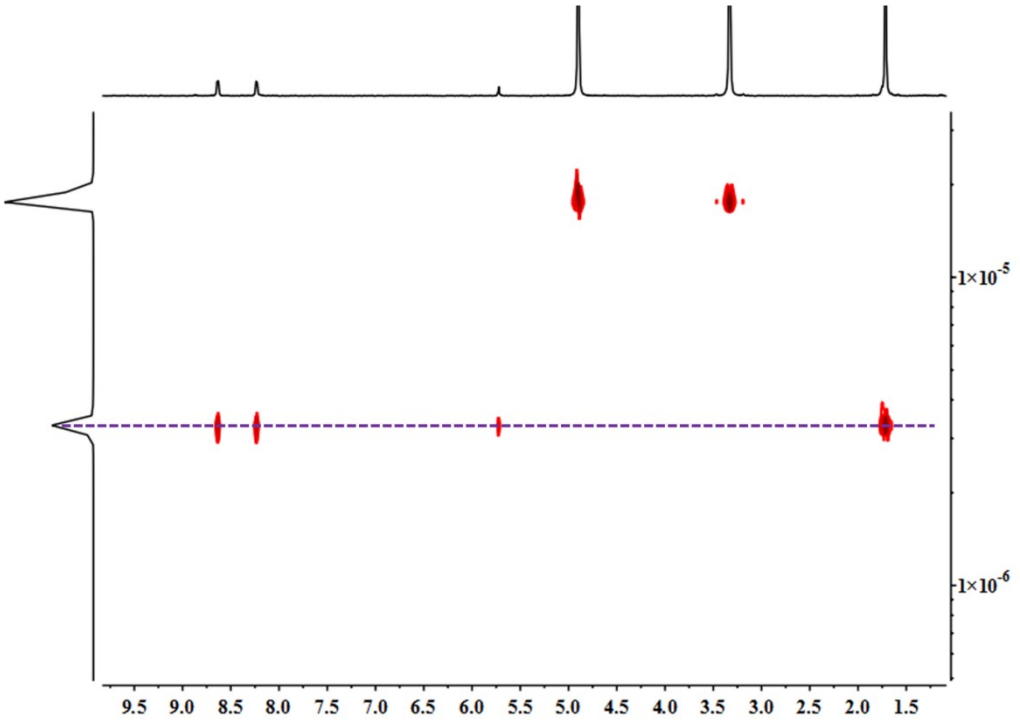

Figure S34. The ^{1}H-^{1}H DOSY NMR (500 MHz, CD_3OD, ppm) for metallarectangle **6** ($D = 3.13 \times 10^{-10}$ m^2s^{-1}, 9.0 mM, with respect to Cp*Rh).

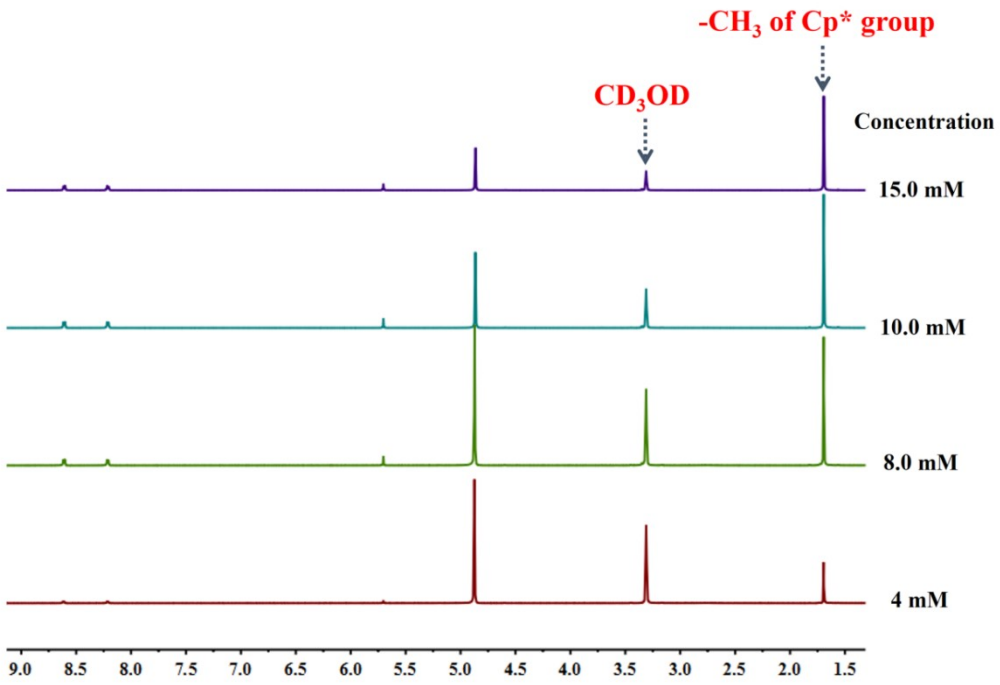

Figure S35. The ^{1}H NMR (500 MHz, CD_3OD, ppm) for metallarectangle **6**, showing high concentration stability of metallarectangle **6.** (4.0-15.0 mM, with respect to Cp*Rh).

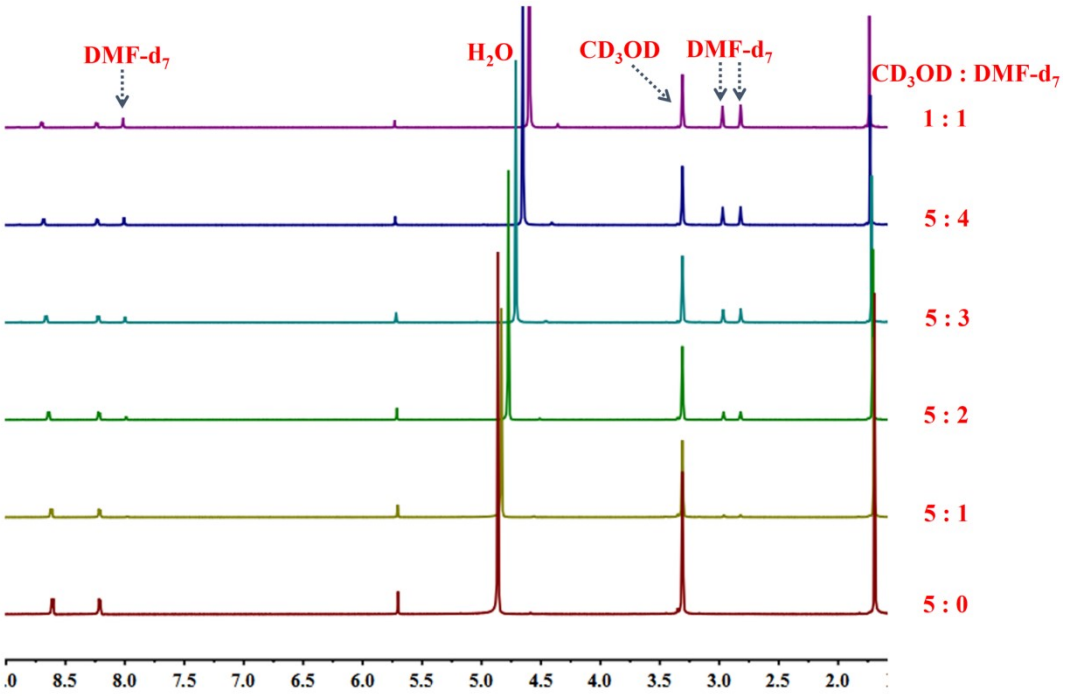

Figure S36. The full ^{1}H NMR spectra for metallarectangle **6**, showing high DMF solvent stability of metallarectangle **6** accompanied by the change of solvent ratio (CD_3OD/DMF-d_7) from 5:0 to 1:1 [10.0 mM, with respect to Cp*Rh], 500 MHz).

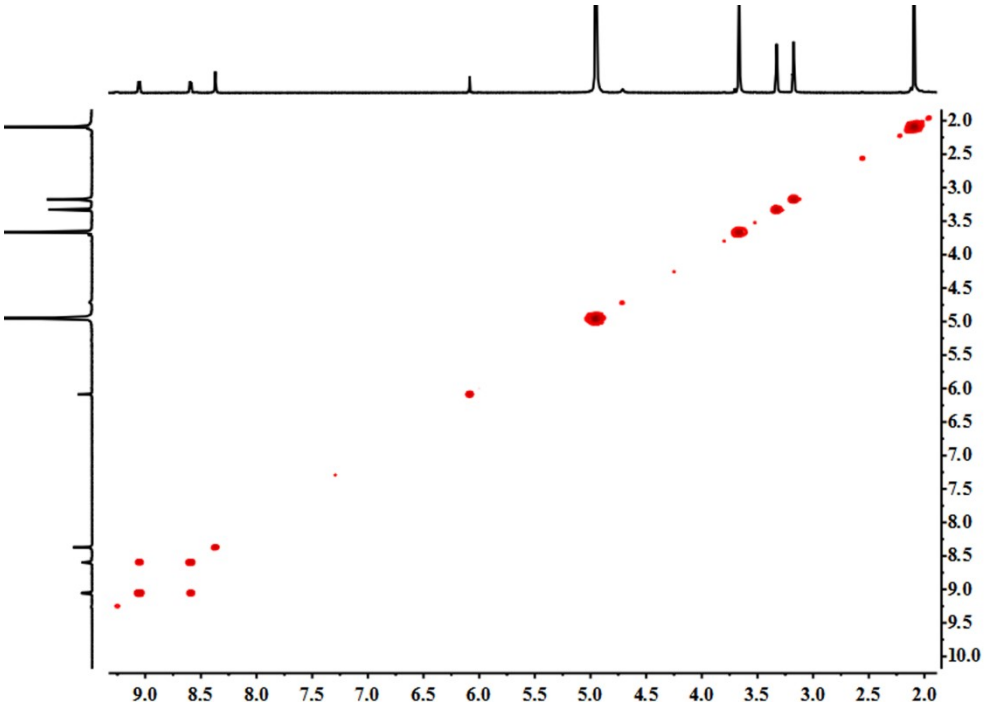

Figure S37. The ^{1}H-^{1}H COSY NMR (500 MHz, CD_3OD, ppm) for metallarectangle **6** in a mixture solution of CD_3OD and DMF-d_7 in a ratio of 1:1 (20.0 mM, with respect to Cp*Rh).

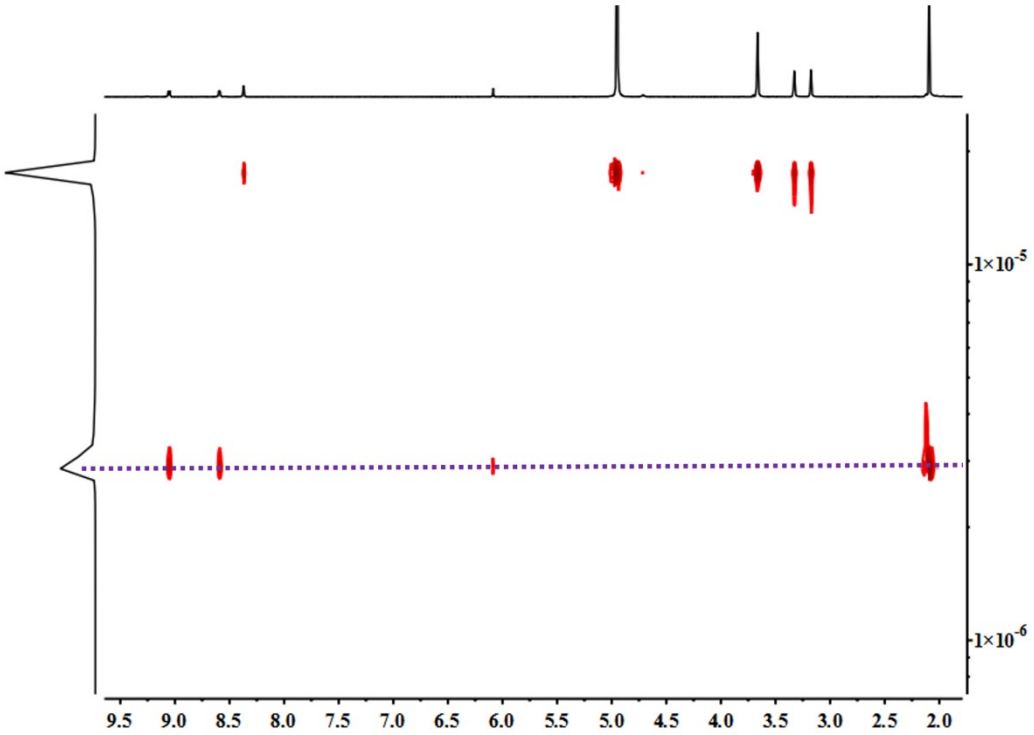

Figure S38. The ^{1}H-^{1}H DOSY NMR (500 MHz, CD_3OD, ppm) for metallarectangle **6** in a mixture solution of CD_3OD and DMF-d_7 in a ratio of 1:1 ($D = 2.95 \times 10^{-10}$ m^2s^{-1}, 20.0 mM, with respect to Cp*Rh).

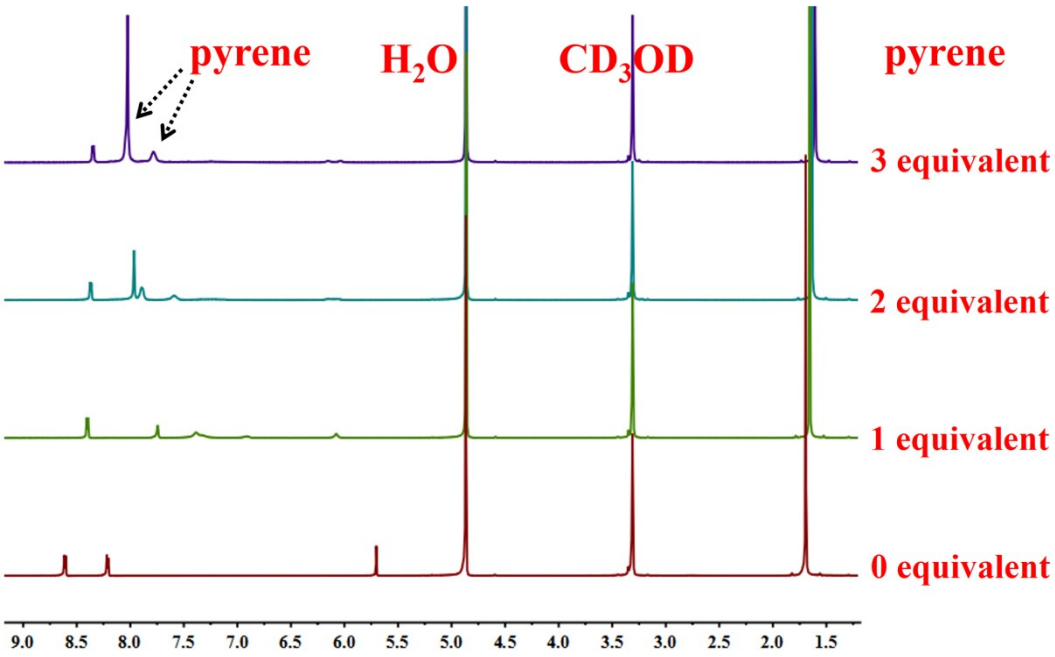

Figure S39. The full ^{1}H NMR spectra for metallarectangle **6**, showing high conjugated molecule stability of metallarectangle **6** accompanied by the increase of pyrene molecules from 0 to three equivalent [10.0 mM, with respect to Cp*Rh], 500 MHz).

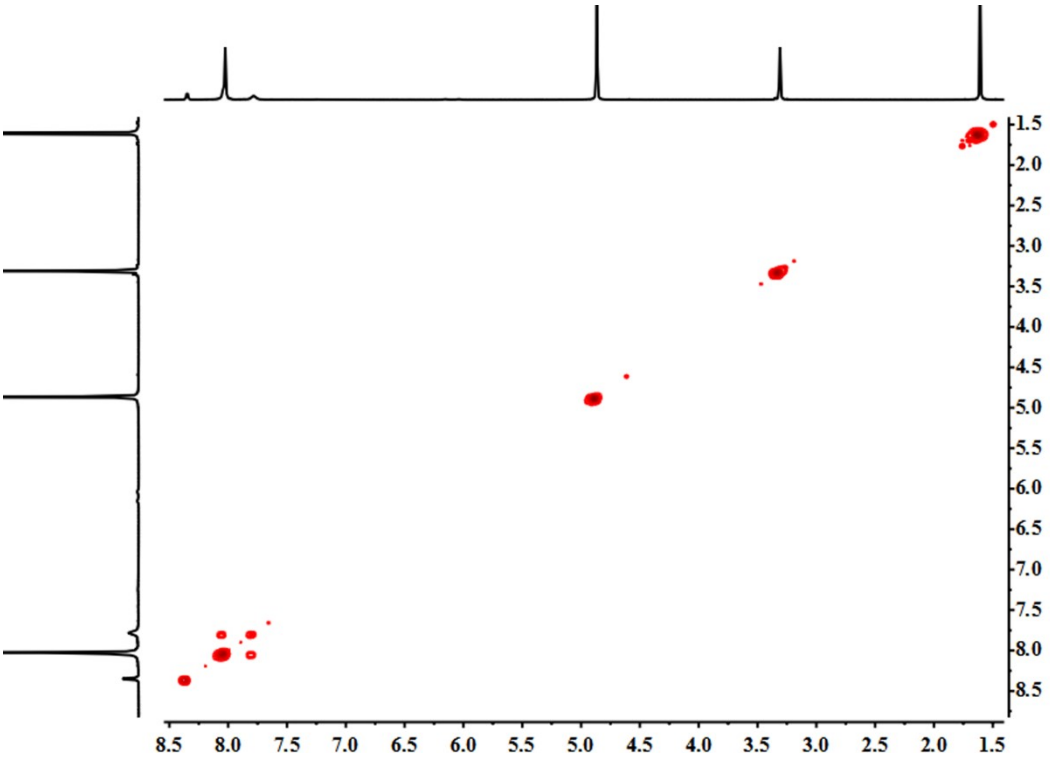

Figure S40. The ^{1}H-^{1}H COSY NMR (500 MHz, CD_3OD, ppm) in a mixture of metallarectangle **6** and three equivalent pyrene molecules (10.0 mM, with respect to Cp*Rh).

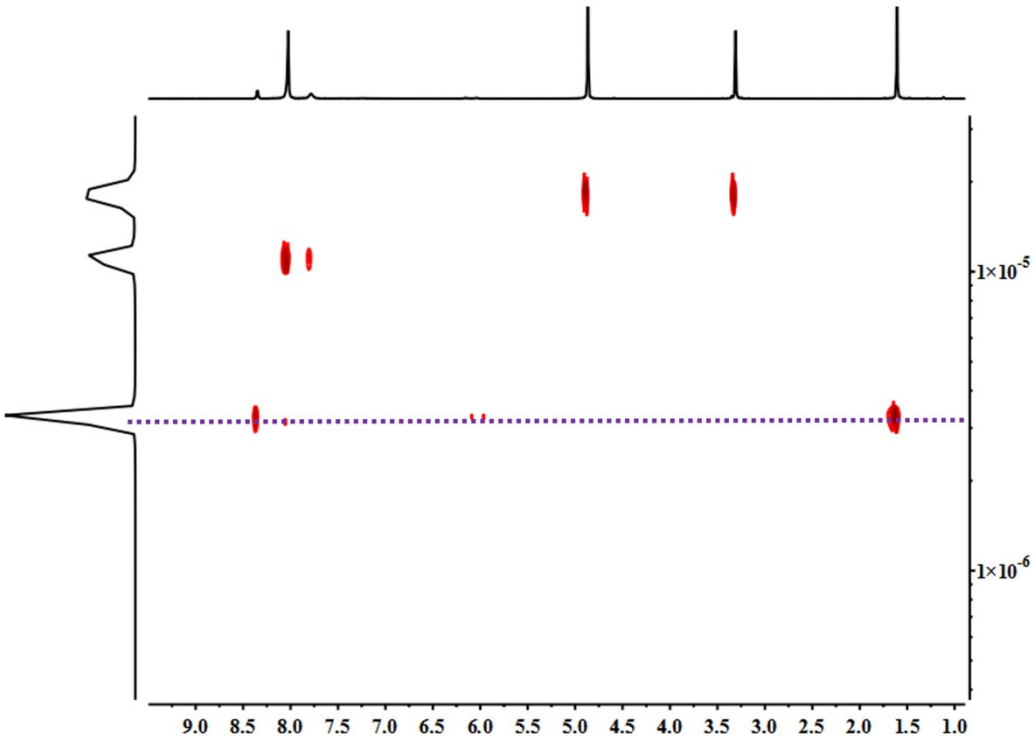

Figure S41. The ^{1}H-^{1}H DOSY NMR (500 MHz, CD_3OD, ppm) in a mixture of metallarectangle **6** and three equivalent pyrene molecules (D = 3.47 × 10^{-10} m^2s^{-1}, 10.0 mM, with respect to Cp*Rh).

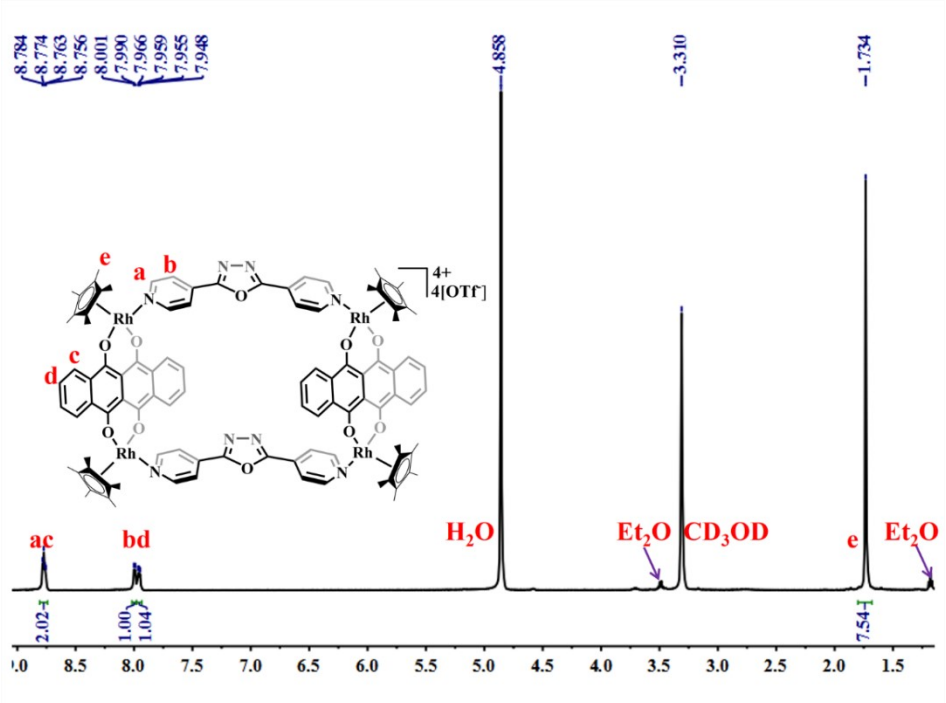

Figure S42. The ^{1}H NMR (500 MHz, CD_3OD, ppm) for metallarectangle **7** (13.0 mM, with respect to Cp*Rh).

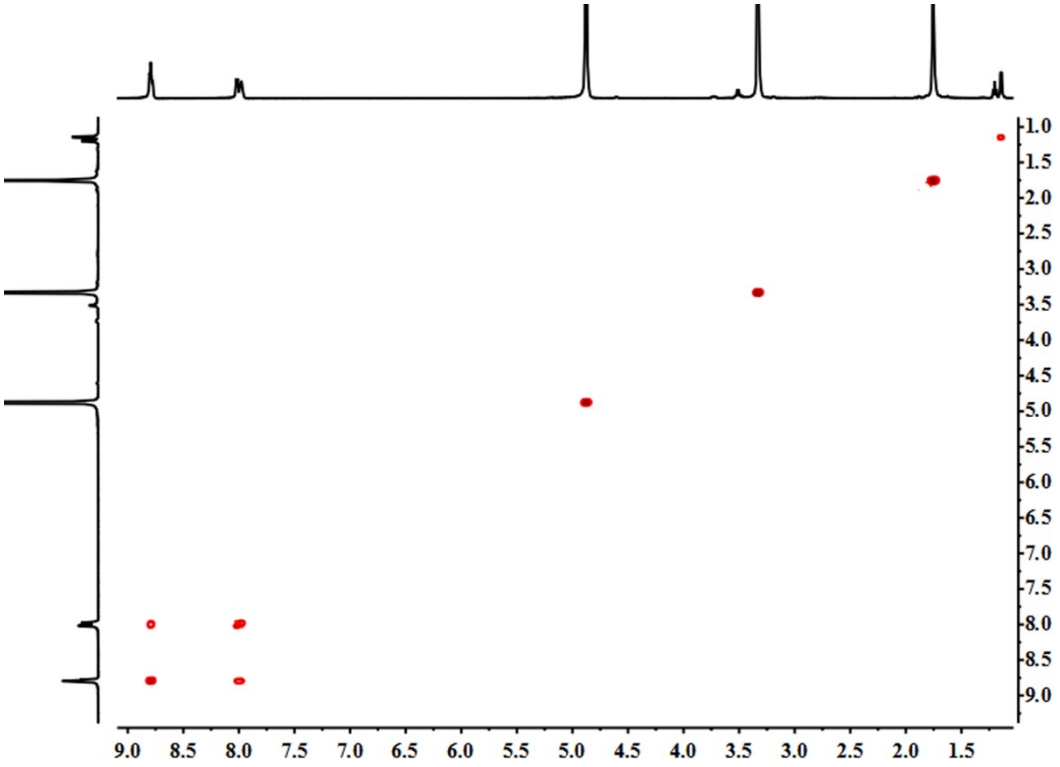

Figure S43. The ^{1}H-^{1}H COSY NMR (500 MHz, CD_3OD, ppm) for metallarectangle **7** (13.0 mM, with respect to Cp*Rh).

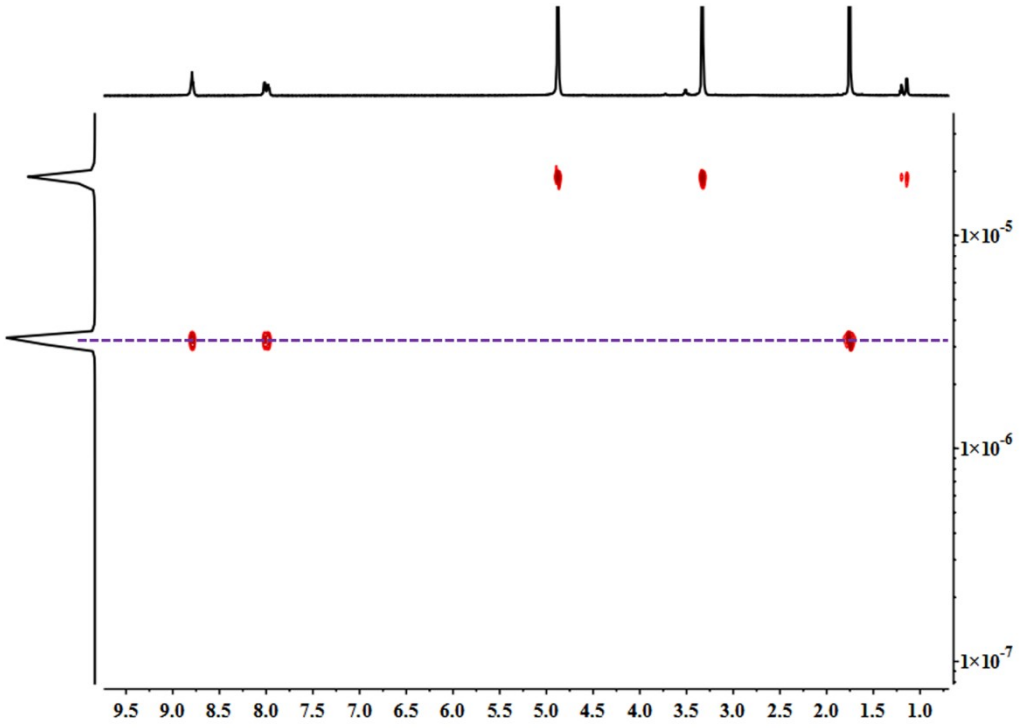

Figure S44. The ^{1}H-^{1}H DOSY NMR (500 MHz, CD_3OD, ppm) for metallarectangle **7** ($D = 3.26 \times 10^{-10}$ m^2s^{-1}, 13.0 mM, with respect to Cp*Rh).

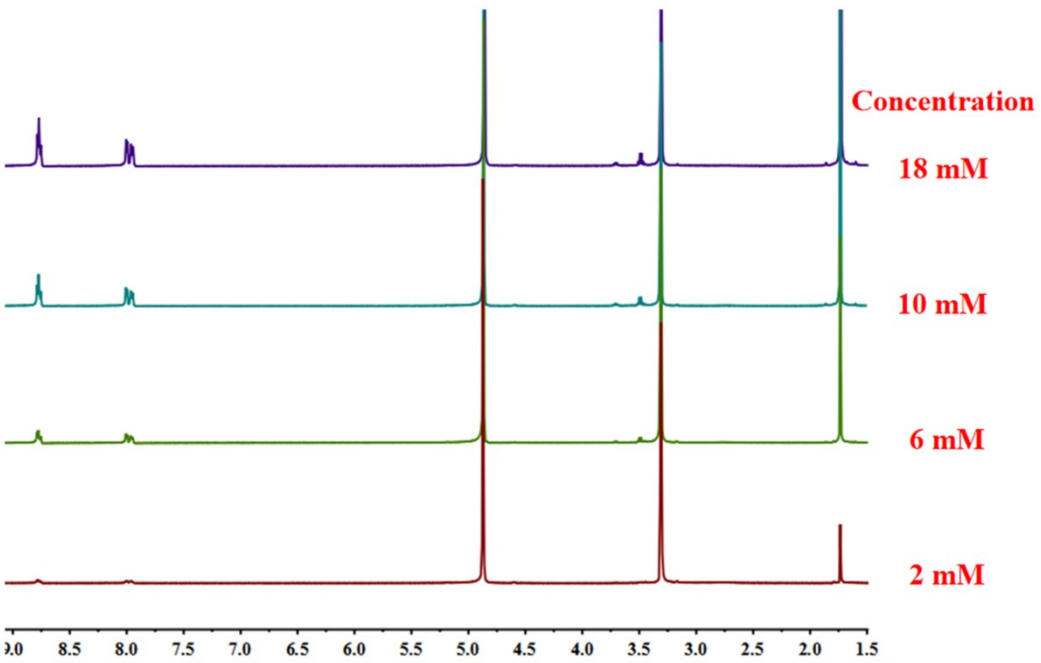

Figure S45. The full ^{1}H NMR spectra for metallarectangle **7**, showing high concentration stability of metallarectangle **7** (2.0-18.0 mM, with respect to Cp*Rh).

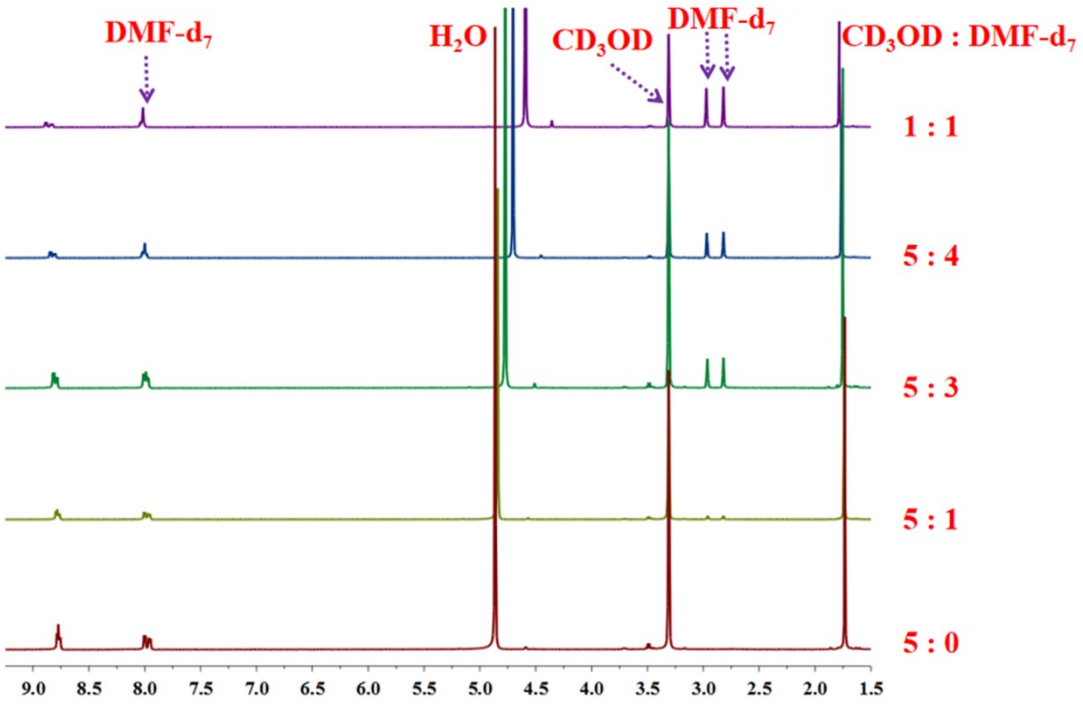

Figure S46. The full ^{1}H NMR spectra for metallarectangle **7**, showing high DMF solvent stability of metallarectangle **7** accompanied by the change of solvent ratio (CD_3OD/DMF-d_7) from 5:0 to 1:1 [13.0 mM, with respect to Cp*Rh], 500 MHz).

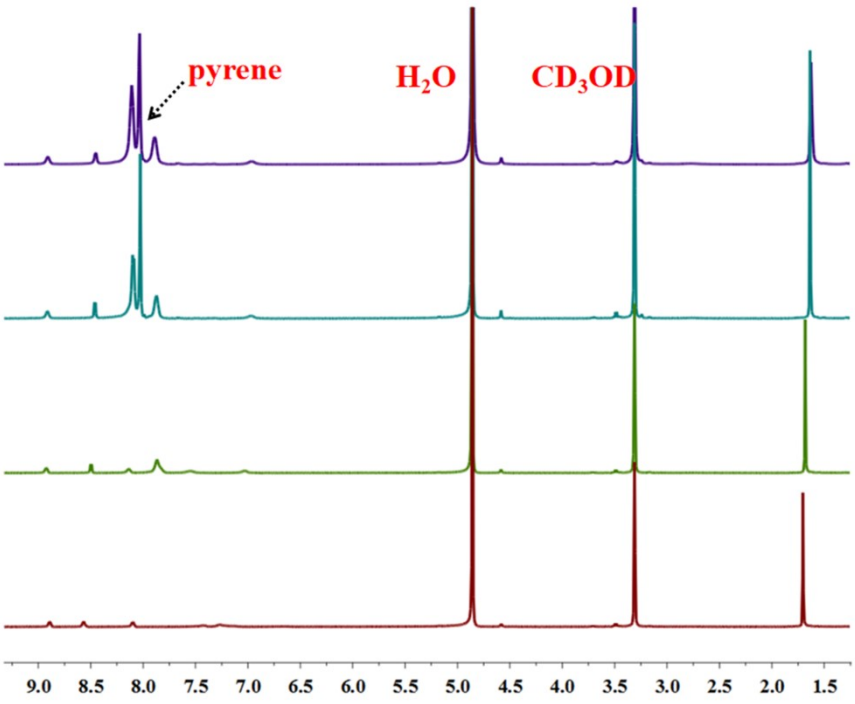

Figure S47. The full ^{1}H NMR spectra for metallarectangle **7**, showing high conjugated molecule stability of metallarectangle **7** accompanied by the increase of pyrene molecules from 0 to three equivalents [13.0 mM, with respect to Cp*Rh], 500 MHz).

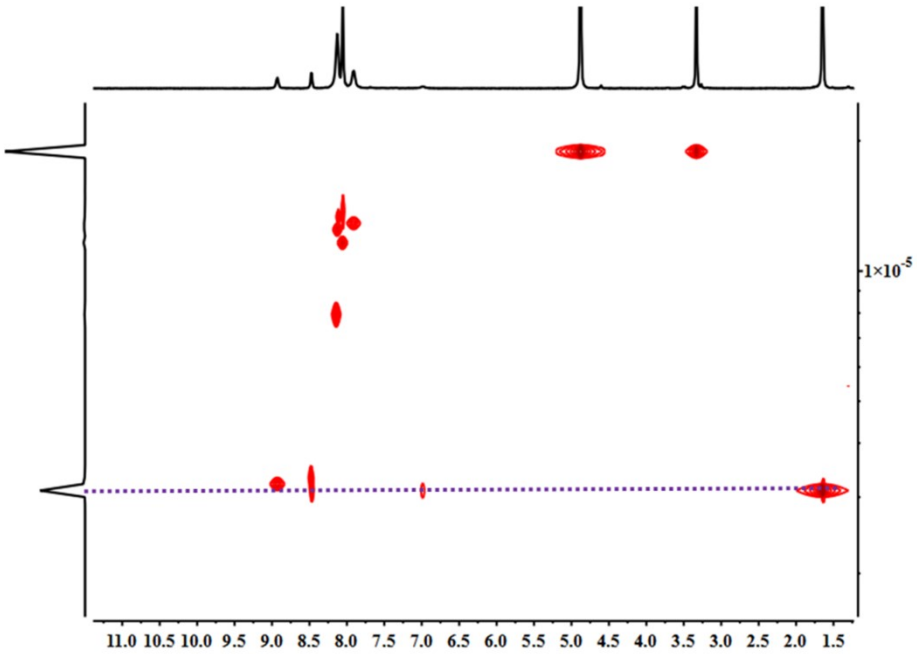

Figure S48. The ^{1}H-^{1}H DOSY NMR (500 MHz, CD_3OD, ppm) for metallarectangle **7** after being added in three equivalents pyrene molecules ($D = 3.19 \times 10^{-10}$ m^2s^{-1}, 13.0 mM, with respect to Cp*Rh).

4. ESI-MS spectra

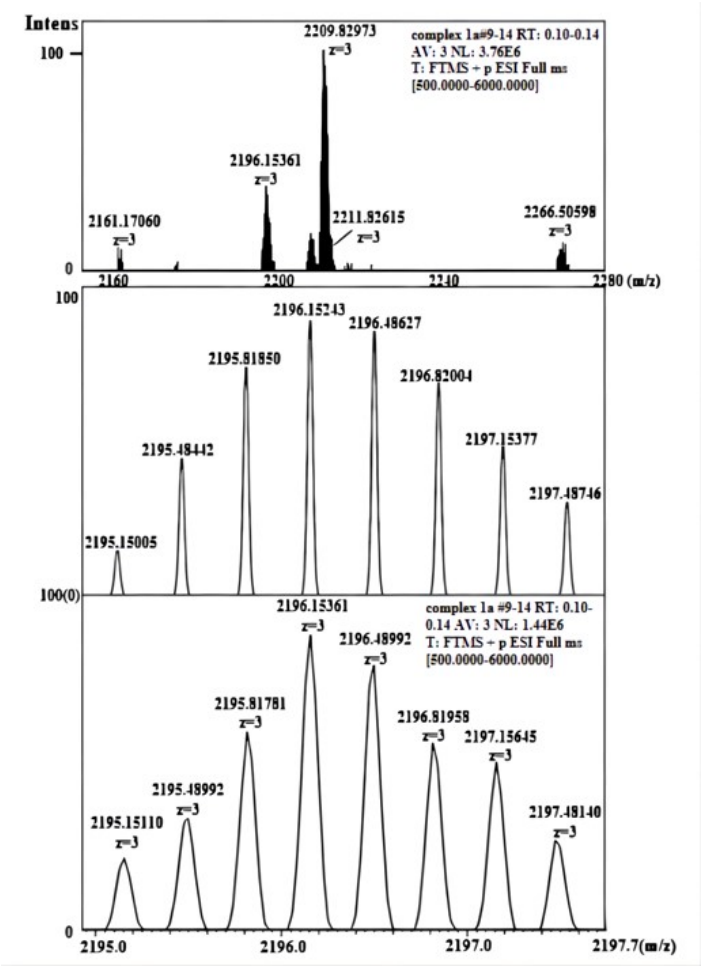

Figure S49. Full ESI-MS spectra (**a**) of Borromean ring **1a**, experimental ESI-MS spectra of $[\mathbf{1a\text{-}3OTf^-}]^{3+}$ in CH_3OH solvent.

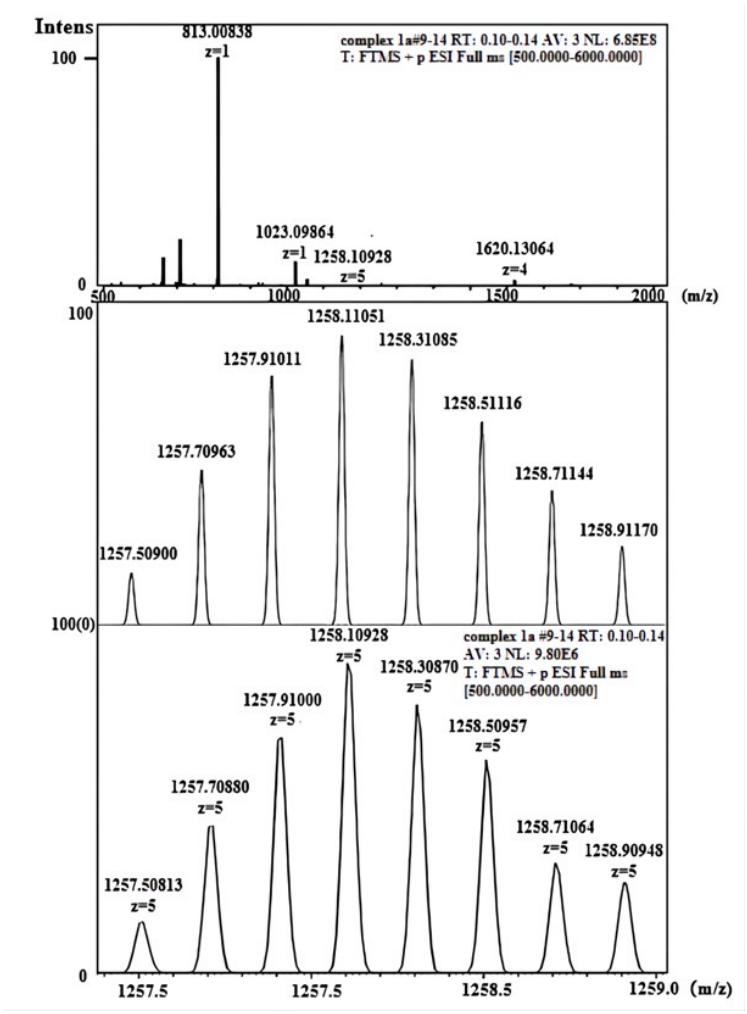

Figure S50. Full ESI-MS spectra (**top**) of complex **1a**, experimental ESI-MS spectra of [**1a-5OTf**$^{-}$]$^{5+}$ in CH_3OH solvent.

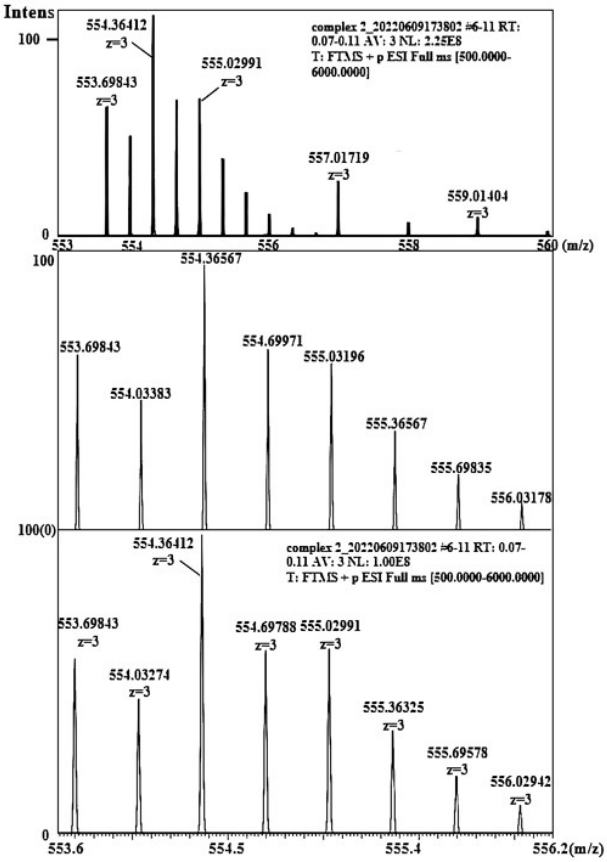

Figure S51. Full ESI-MS spectra (**a**) of complex **2**, experimental ESI-MS spectra of [**2-3OTf**$^{-}$**]**$^{3+}$ in CH_3OH solvent.

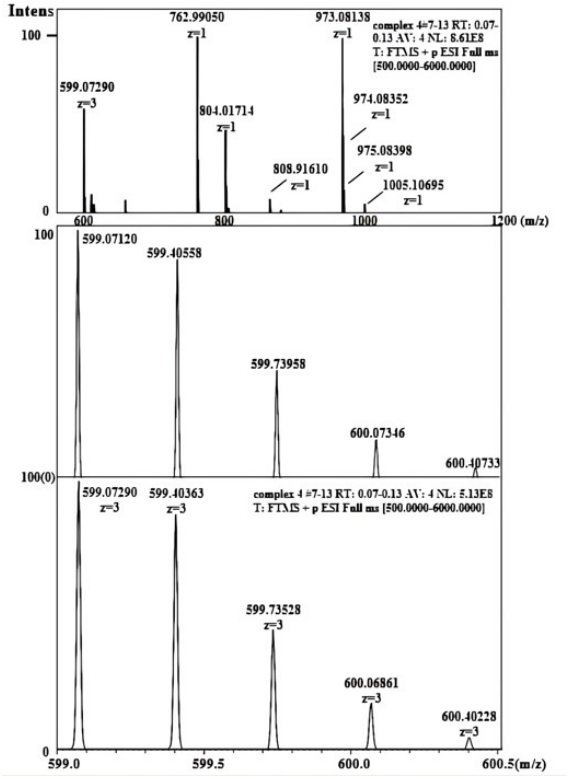

Figure S52. Full ESI-MS spectra (**a**) of complex **4**, experimental ESI-MS spectra of [**4-3OTf**$^{-}$**]**$^{3+}$ in CH_3OH solvent.

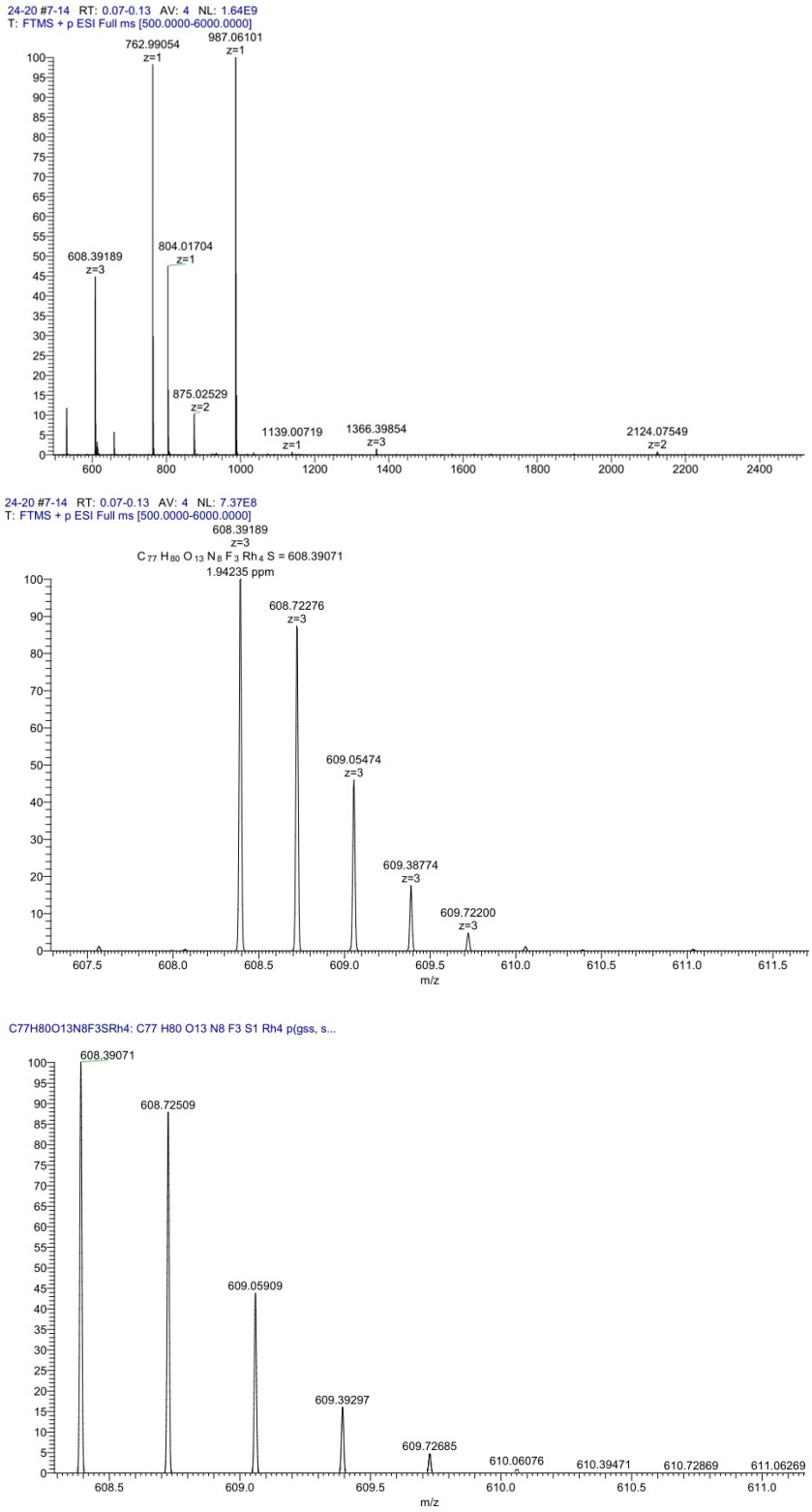

Figure S53. Full ESI-MS spectra (Top) of complex **6**, experimental ESI-MS spectra of $[\mathbf{6\text{-}3OTf^-}]^{3+}$ in CH_3OH solvent.

5. The UV-vis spectra

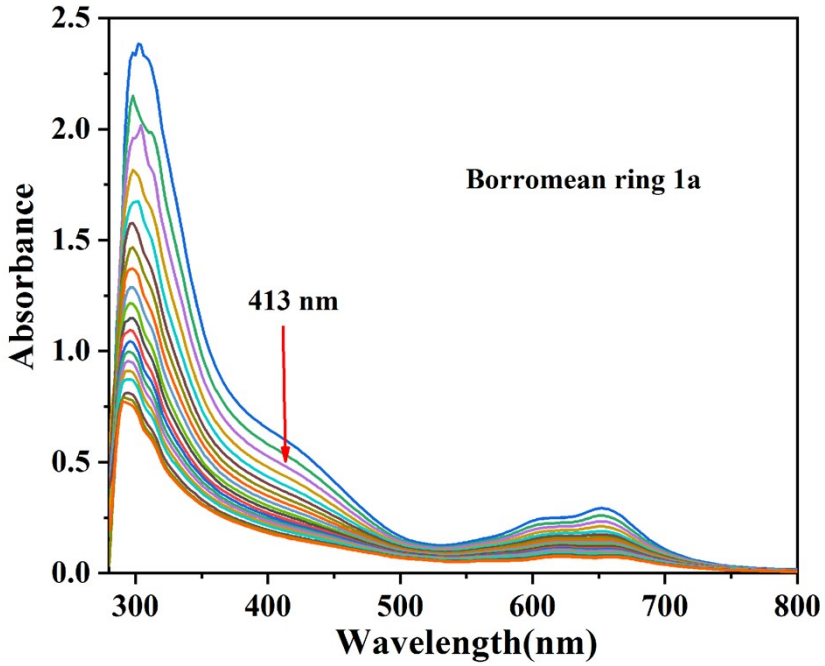

Figure S54. The full UV/vis spectra of Borromean ring **1a** accompanied by the dilution process from 3.5 mM to 0.2 mM in CH_3CN.

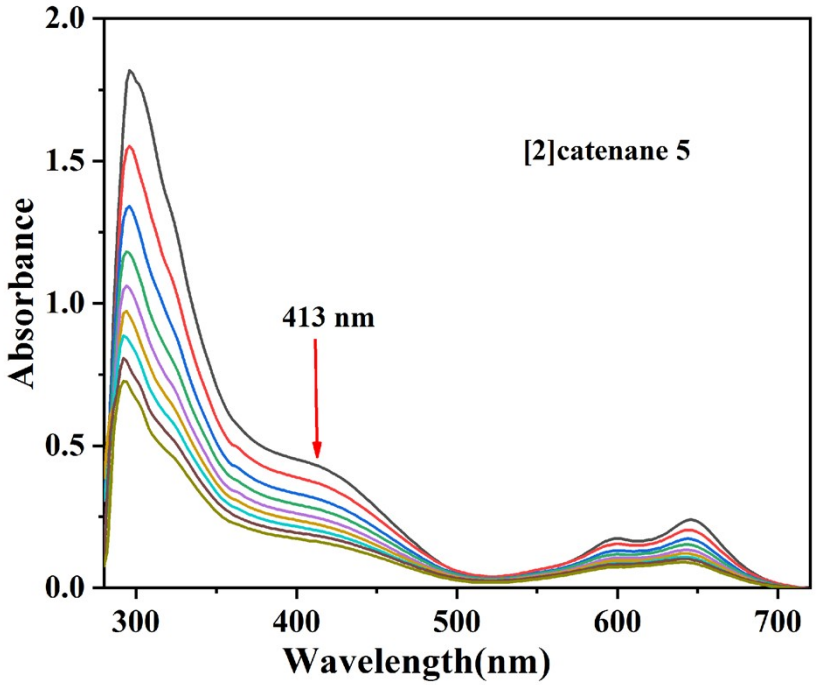

Figure S55. The full UV/vis spectra of [2]catenane **5** accompanied by the dilution process from 5.0 mM to 0.25 mM in CH_3CN.

6. Near-infrared photothermal conversion research

1. Experimental details.

(a) Details in solution.

To guarantee same amount of conjugated - π area, the applied molar ratio of the four topologies **1a**/**2**/**3**/**4**/**5**/**6**/**7** was 2:6:6:6:3:6:6. Complex **1a** (1.40 mg, 0.0002mmol) was added into a solvent of CH_3OH (5.0 ml). After the solid dissolved absolutely, 3.0 ml of this solution was taken into quartz spectrophotometer cell (1×1×5 cm) and put into the bright spot of a laser with 660 nm wavelength at different current intensities. Temperature variation of the solution was detected by an infrared camera. Complex **2** (1.10 mg, 0.0005 mmol), Complex **3** (1.10 mg, 0.0005 mmol) and Complex **4** (1.15 mg, 0.0005 mmol), Complex **5** (1.21 mg, 0.0003 mmol), Complex **6** (1.20 mg, 0.0005 mmol) and Complex **7** (1.30 mg, 0.0005 mmol), were detected with the same procedure as complex **1a**.

(b) Details in the liquid state.

The methanol solution in **(a)** each contained complex **1a,** complex **2,** complex **3,** complex **4,** complex **5,** complex **6,** and complex **7** were put a 0.7ml sample vessel. And then, they were put under a laser and temperature variation were detected by a same infrared camera. Equations used to calculate near-infrared photothermal conversion efficiency were exhibited as follows:

$$\eta = hS(\Delta T_{sample} - \Delta T_{solvent}) / I(1-10^{-A}) \quad (1)$$

$$hS = \sum mC_p/\tau_s \quad (2)$$

$$\tau_s = -t/\ln\theta \quad (3)$$

$$\theta = (T_{amb} - T)/(T_{amb} - T_{max}) \quad (4)$$

Thereinto, C_p=2.51 KJ/(Kg • K), $\Delta T_{solvent}$ = 2.2℃. **I** = 0.6 W/cm^2, **h** is the heat transfer coefficient and **S** is the surface area of the container. τ_s is the sample system time constant, m is the mass of the products,Thus, $\sum mC_p = m_{(methanol)} C_{p(methanol)} = \rho_{(methanol)} V_{(methanol)} C_{p(methanol)} = 0.791 \times 0.7 \times 2.51 = 1.3898\ J \cdot K^{-1}$.

Here, the volume deviation of the mixed solvent is ignored.

2. Complex 1a (Borromean ring).

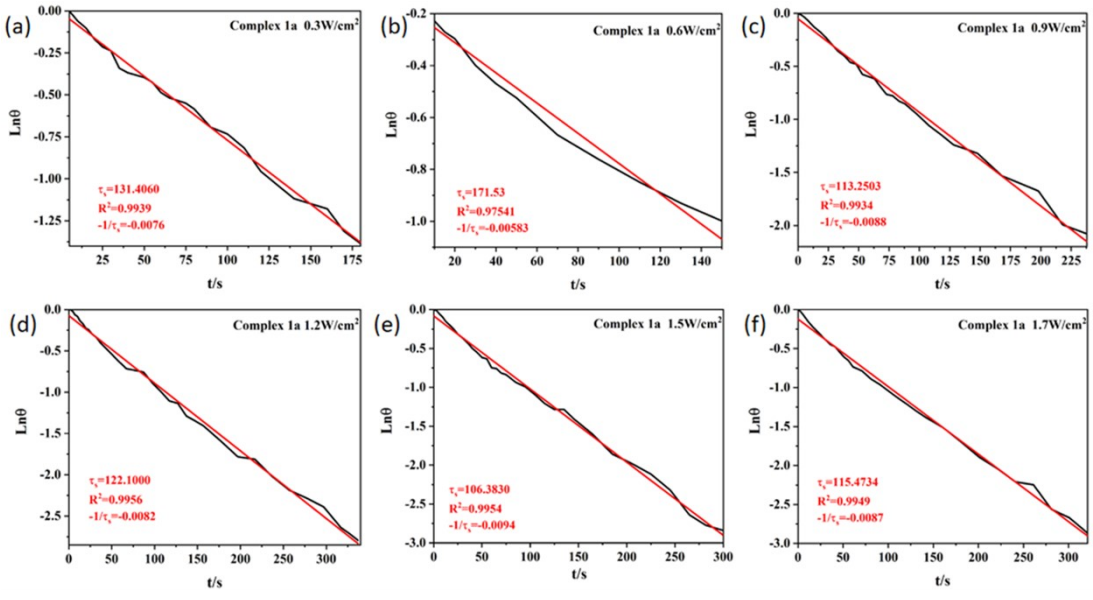

Figure S56. The complex **1a** in methanol under laser irradiation of different current intensities was ploted it as the Fitting linear of lnθ-t.

Near-infrared photothermal conversion efficiency η of **1a** was calculated by equations above. A fitting linear of lnθ-t was obtained by Eqs (3) and (4), by which η was calculated as 11.8 %, 19.72 %, 23.58 %, 18.54 %,19.76 % and 17.81 % at different laser power densities of 0.5, 0.7, 0.9, 1.1, 1.3, and 1.5 W/cm^{-2}.

3. Complex 5 ([2]catenane)

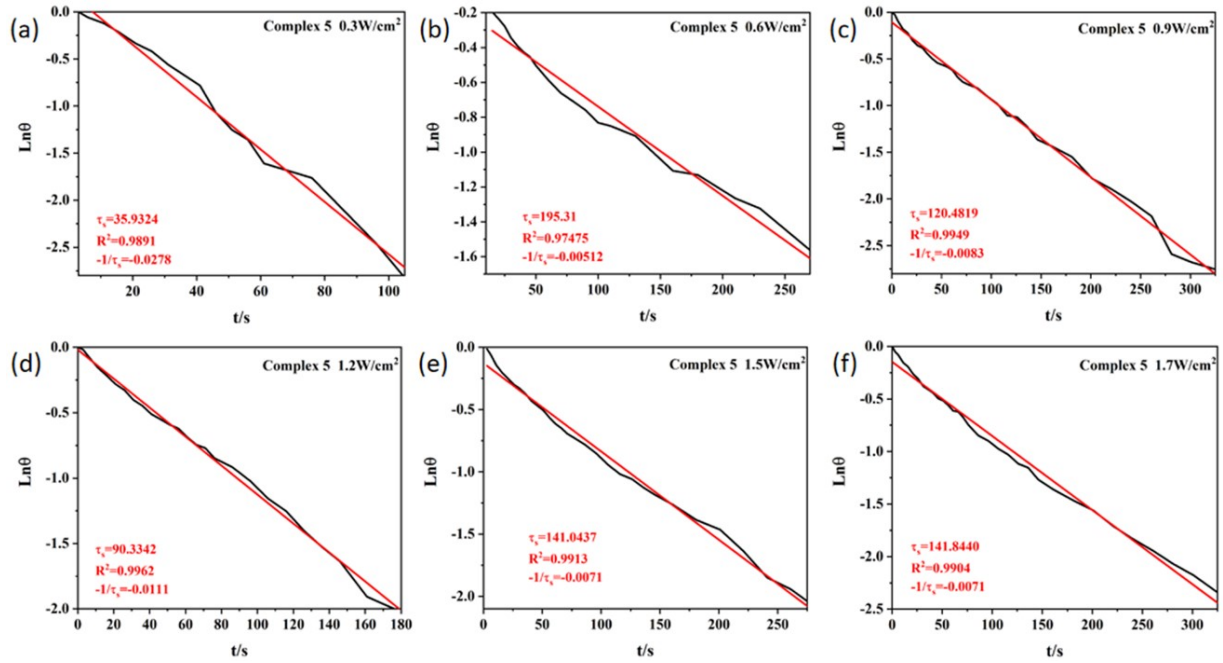

Figure S57. The complex **5 ([2]catenane)** in methanol under laser irradiation of different current intensities was ploted it as the Fitting linear of lnθ-t.

Near-infrared photothermal conversion efficiency η of **5** was calculated by equations above. A fitting linear of lnθ-t was obtained by Eqs (3) and (4), by which η was calculated as 18.82 %, 14.84 %, 19.86 %, 22.03 %,14.31 % and 13.98 % at different laser power densities of 0.5, 0.7, 0.9, 1.1, 1.3, and 1.5 W/cm^{-2}.

7. X-ray crystallography details

Single crystals of **1a**, **2**, **3**, **4**, **5**, **6** and **7**, suitable for X-ray diffraction study were obtained at room temperature. X-ray intensity data of them were collected at 250, 173, 150, 173, 150, 173 K and 193K on a CCD-Bruker SMART APEX system. In these data, the disordered solvent molecules which could not be restrained properly were removed using the PLATON Squeeze routine.

In asymmetric unit of **1a**, a solvent mask was calculated and 3068 electrons were found in a volume of 9729\%A^3^ in 5 voids per unit cell. This is consistent with the presence of 0.9[CH3OH], 10[CF3SO3], 0.7[CH3OH], 0.9[CH3OH] per Asymmetric Unit which account for 3100 electrons per unit cell.
In asymmetric unit of **2**， A solvent mask was calculated and 402 electrons were found in a volume of 2750\%A^3^ in 1 void per unit cell. This is consistent with the presence of 0.088[C6H14O] per Asymmetric Unit which account for 464 electrons per unit cell.
In asymmetric unit of **3**, a solvent mask was calculated and 138 electrons were found in a volume of 540\%A^3^ in 1 void per unit cell. This is consistent with the presence of 8[CH3OH] per Asymmetric Unit which account for 144 electrons per unit cell.
In asymmetric unit of **4**, a solvent mask was calculated and 86 electrons were found in a volume of 572\%A^3^ in 2 voids per unit cell. This is consistent with the presence of 1.3[CH3OH] per Asymmetric Unit which account for 94 electrons per unit cell.
In asymmetric unit of **5**, a solvent mask was calculated and 1758 electrons were found in a volume of 6008\%A^3^ in 3 voids per unit cell. This is consistent with the presence of 0.5[CH3OH], 6[CF3SO3], 0.9[CH3OH] per Asymmetric Unit which account for 1853 electrons per unit cell.
In asymmetric unit of **6**, a solvent mask was calculated and 426 electrons were found in a volume of 1196\%A^3^ in 1 void per unit cell. This is consistent with the presence of 1.5[CF3SO3] per Asymmetric Unit which account for 438 electrons per unit cell.
In asymmetric unit of **7**, a solvent mask was calculated and 772 electrons were found in a volume of 4744\%A^3^ in 2 voids per unit cell. This is consistent with the presence of 0.3[CH3OH], 3.4[C6H14O] per Asymmetric Unit which account for 810 electrons per unit cell.

Table 1 Crystal data and structure refinement for 1a.

Empirical formula	$C_{543}F_{96}H_{546}N_{48}O_{149}Rh_{24}S_{32}$
Formula weight	15448.00
Temperature/K	193.00
Crystal system	monoclinic
Space group	P21/c
a/Å	39.606(3)
b/Å	22.0684(15)
c/Å	40.033(3)
α/°	90
β/°	112.497(3)
γ/°	90
Volume/Å3	32328(4)
Z	2
ρcalcg/cm3	1.587
μ/mm-1	4.505
F(000)	15576.0
Crystal size/mm3	0.2 × 0.17 × 0.15
Radiation	GaKα (λ = 1.34139)
2Θ range for data collection/°	3.874 to 108.336
Index ranges	-47 ≤ h ≤ 46, -26 ≤ k ≤ 26, -47 ≤ l ≤ 48
Reflections collected	250412
Independent reflections	59375 [Rint = 0.1082, Rsigma = 0.0877]
Data/restraints/parameters	59375/5731/3243
Goodness-of-fit on F2	1.019
Final R indexes [I>=2σ (I)]	R1 = 0.0957, wR2 = 0.2804
Final R indexes [all data]	R1 = 0.1659, wR2 = 0.3364
Largest diff. peak/hole / e Å-3	1.88/-1.49

Table 2 Crystal data and structure refinement for 2.

Empirical formula	$C_{80}C_{l4}F_{12}H_{28}N_8O_{14}Rh_4S_4$
Formula weight	2234.78
Temperature/K	193.00
Crystal system	tetragonal
Space group	*P*42/n
a/Å	28.6327(10)
b/Å	28.6327(10)
c/Å	12.2481(6)
α/°	90
β/°	90
γ/°	90
Volume/Å3	10041.4(9)
Z	4
ρcalcg/cm3	1.478
μ/mm-1	5.163
F(000)	4384.0
Crystal size/mm3	0.24 × 0.22 × 0.2
Radiation	GaKα (λ = 1.34139)
2Θ range for data collection/°	5.37 to 107.828
Index ranges	-34 ≤ h ≤ 34, -34 ≤ k ≤ 30, -14 ≤ l ≤ 14
Reflections collected	74353
Independent reflections	9152 [Rint = 0.0445, Rsigma = 0.0260]
Data/restraints/parameters	9152/487/515
Goodness-of-fit on F2	1.061
Final R indexes [I>=2σ (I)]	R1 = 0.0428, wR2 = 0.1315
Final R indexes [all data]	R1 = 0.0517, wR2 = 0.1377
Largest diff. peak/hole / e Å-3	0.57/-1.13

Table 3 Crystal data and structure refinement for 3.

Empirical formula	$C_{80}F_{12}H_{112}N_8O_{28}Rh_4S_4$
Formula weight	2401.65
Temperature/K	149.99(10)
Crystal system	triclinic
Space group	P-1
a/Å	12.2741(4)
b/Å	14.5553(6)
c/Å	15.9583(6)
α/°	114.615(4)
β/°	97.597(3)
γ/°	101.737(3)
Volume/Å3	2461.21(18)
Z	1
ρcalcg/cm3	1.620
μ/mm-1	0.844
F(000)	1224.0
Crystal size/mm3	0.24 × 0.22 × 0.2
Radiation	Mo Kα (λ = 0.71073)
2Θ range for data collection/°	4.572 to 50
Index ranges	-13 ≤ h ≤ 14, -16 ≤ k ≤ 17, -18 ≤ l ≤ 18
Reflections collected	16583
Independent reflections	8668 [Rint = 0.0293, Rsigma = 0.0533]
Data/restraints/parameters	8668/560/551
Goodness-of-fit on F2	1.030
Final R indexes [I>=2σ (I)]	R1 = 0.0818, wR2 = 0.2237
Final R indexes [all data]	R1 = 0.0964, wR2 = 0.2397
Largest diff. peak/hole / e Å-3	4.26/-2.56

Table 4 Crystal data and structure refinement for 4.

Empirical formula	$C_{80}H_{84}F_{12}N_8O_{20}Rh_4S_4$
Formula weight	2245.43
Temperature/K	193.00
Crystal system	monoclinic
Space group	P21/c
a/Å	14.2991(8)
b/Å	9.2719(5)
c/Å	36.5863(17)
α/°	90
β/°	98.401(3)
γ/°	90
Volume/Å3	4798.6(4)
Z	2
ρcalcg/cm3	1.554
μ/mm-1	4.758
F(000)	2264.0
Crystal size/mm3	0.2 × 0.18 × 0.16
Radiation	GaKα (λ = 1.34139)
2Θ range for data collection/°	4.248 to 107.922
Index ranges	-17 ≤ h ≤ 17, -11 ≤ k ≤ 6, -44 ≤ l ≤ 23
Reflections collected	32754
Independent reflections	8748 [Rint = 0.0743, Rsigma = 0.0661]
Data/restraints/parameters	8748/575/587
Goodness-of-fit on F2	1.022
Final R indexes [I>=2σ (I)]	R1 = 0.0735, wR2 = 0.2054
Final R indexes [all data]	R1 = 0.1101, wR2 = 0.2338
Largest diff. peak/hole / e Å-3	2.24/-1.16

Table 5 Crystal data and structure refinement for 5

Empirical formula	$C_{180.4}F_{33}H_{173.6}N_{16}O_{54.4}Rh_8S_{11}$
Formula weight	5239.08
Temperature/K	193.00
Crystal system	monoclinic
Space group	P21/c
a/Å	35.8023(15)
b/Å	16.7153(8)
c/Å	36.5538(17)
α/°	90
β/°	98.060(2)
γ/°	90
Volume/Å3	21659.4(17)
Z	4
ρcalcg/cm3	1.607
μ/mm-1	4.525
F(000)	10545.0
Crystal size/mm3	0.25 × 0.22 × 0.2
Radiation	GaKα (λ = 1.34139)
2Θ range for data collection/°	2.814 to 120.838
Index ranges	-45 ≤ h ≤ 40, -18 ≤ k ≤ 21, -46 ≤ l ≤ 36
Reflections collected	164579
Independent reflections	47800 [Rint = 0.0689, Rsigma = 0.0711]
Data/restraints/parameters	47800/2405/2308
Goodness-of-fit on F2	1.071
Final R indexes [I>=2σ (I)]	R1 = 0.0774, wR2 = 0.2194
Final R indexes [all data]	R1 = 0.1155, wR2 = 0.2466
Largest diff. peak/hole / e Å-3	1.47/-0.73

Table 6 Crystal data and structure refinement for 6

Empirical formula	$C_{81}F_{15}H_{80}N_8O_{25}Rh_4S_5$
Formula weight	2422.47
Temperature/K	193.00
Crystal system	monoclinic
Space group	P21/c
a/Å	14.3226(9)
b/Å	9.2264(5)
c/Å	36.521(2)
α/°	90
β/°	92.038(3)
γ/°	90
Volume/Å3	4823.0(5)
Z	2
ρcalcg/cm3	1.668
μ/mm-1	4.952
F(000)	2434.0
Crystal size/mm3	0.21 × 0.2 × 0.16
Radiation	GaKα (λ = 1.34139)
2Θ range for data collection/°	5.372 to 108.07
Index ranges	-15 ≤ h ≤ 17, -8 ≤ k ≤ 11, -44 ≤ l ≤ 44
Reflections collected	30284
Independent reflections	8783 [Rint = 0.0472, Rsigma = 0.0476]
Data/restraints/parameters	8783/11/543
Goodness-of-fit on F2	1.074
Final R indexes [I>=2σ (I)]	R1 = 0.0441, wR2 = 0.1142
Final R indexes [all data]	R1 = 0.0592, wR2 = 0.1226
Largest diff. peak/hole / e Å-3	0.68/-1.08

Table 7 Crystal data and structure refinement for 7

Empirical formula	$C_{124.7}F_{12}H_{140.8}N_8O_{25.7}Rh_4S_4$
Formula weight	2930.72
Temperature/K	193.00
Crystal system	orthorhombic
Space group	Pnma
a/Å	38.9323(13)
b/Å	29.3060(10)
c/Å	12.4311(4)
α/°	90
β/°	90
γ/°	90
Volume/Å3	14183.3(8)
Z	4
ρcalcg/cm3	1.372
μ/mm-1	3.324
F(000)	6010.0
Crystal size/mm3	0.17 × 0.16 × 0.14
Radiation	GaKα (λ = 1.34139)
2Θ range for data collection/°	3.948 to 107.96
Index ranges	-46 ≤ h ≤ 46, -26 ≤ k ≤ 35, -12 ≤ l ≤ 14
Reflections collected	89968
Independent reflections	13228 [Rint = 0.0501, Rsigma = 0.0320]
Data/restraints/parameters	13228/682/700
Goodness-of-fit on F2	1.059
Final R indexes [I>=2σ (I)]	R1 = 0.0923, wR2 = 0.2263
Final R indexes [all data]	R1 = 0.1003, wR2 = 0.2305
Largest diff. peak/hole / e Å-3	2.44/-0.82

8. References

1. C. White, A. Yates and P. M. Maitlis, *η*5 -Pentamethylcyclopentadienyl) rhodium and -iridium

compounds. *Inorg. Synth*., **1992**, *29*, 228–234.

2. T. Wu, L. H. Weng and G. X. Jin, Sunlight induced cycloaddition and host–guest property of self-assembled organometallic macrocycles based on a versatile building block. *Chem. Comm*., **2012**, *48*, 4435–4437.